

AWARD NUMBER: W81XWH-16-1-0401

TITLE: Powering Up Mitochondrial Functions to Treat Mitochondrial Disease

PRINCIPAL INVESTIGATOR: Douglas Wallace, Ph.D.

CONTRACTING ORGANIZATION: Children's Hospital of Philadelphia Research Institute  
Philadelphia, PA 19104

REPORT DATE: October 2018

TYPE OF REPORT: Annual

PREPARED FOR: U.S. Army Medical Research and Materiel Command  
Fort Detrick, Maryland 21702-5012

DISTRIBUTION STATEMENT: Approved for Public Release;  
Distribution Unlimited

The views, opinions and/or findings contained in this report are those of the author(s) and should not be construed as an official Department of the Army position, policy or decision unless so designated by other documentation.

# REPORT DOCUMENTATION PAGE

*Form Approved*  
**OMB No. 0704-0188**

Public reporting burden for this collection of information is estimated to average 1 hour per response, including the time for reviewing instructions, searching existing data sources, gathering and maintaining the data needed, and completing and reviewing this collection of information. Send comments regarding this burden estimate or any other aspect of this collection of information, including suggestions for reducing this burden to Department of Defense, Washington Headquarters Services, Directorate for Information Operations and Reports (0704-0188), 1215 Jefferson Davis Highway, Suite 1204, Arlington, VA 22202-4302. Respondents should be aware that notwithstanding any other provision of law, no person shall be subject to any penalty for failing to comply with a collection of information if it does not display a currently valid OMB control number. **PLEASE DO NOT RETURN YOUR FORM TO THE ABOVE ADDRESS.**

<b>1. REPORT DATE</b> October 2018			<b>2. REPORT TYPE</b> Annual			<b>3. DATES COVERED</b> 30 Sep 2017 - 29 Sep 2018			
<b>4. TITLE AND SUBTITLE</b>  Powering Up Mitochondrial Functions to Treat Mitochondrial Disease						<b>5a. CONTRACT NUMBER</b>			
						<b>5b. GRANT NUMBER</b> W81XWH-16-1-0401			
						<b>5c. PROGRAM ELEMENT NUMBER</b>			
<b>6. AUTHOR(S)</b> Douglas C. Wallace, Ph.D. and Liming Pei, Ph.D.  E-Mail: wallaced1@email.chop.edu and peil@email.chop.edu						<b>5d. PROJECT NUMBER</b>			
						<b>5e. TASK NUMBER</b>			
						<b>5f. WORK UNIT NUMBER</b>			
<b>7. PERFORMING ORGANIZATION NAME(S) AND ADDRESS(ES)</b> Children's Hospital of Philadelphia, The 3615 Civic Center Blvd Philadelphia, PA 19104-4318						<b>8. PERFORMING ORGANIZATION REPORT NUMBER</b>			
<b>9. SPONSORING / MONITORING AGENCY NAME(S) AND ADDRESS(ES)</b>  U.S. Army Medical Research and Materiel Command Fort Detrick, Maryland 21702-5012						<b>10. SPONSOR/MONITOR'S ACRONYM(S)</b>			
						<b>11. SPONSOR/MONITOR'S REPORT NUMBER(S)</b>			
<b>12. DISTRIBUTION / AVAILABILITY STATEMENT</b>  Approved for Public Release; Distribution Unlimited									
<b>13. SUPPLEMENTARY NOTES</b>									
<b>14. ABSTRACT</b> We proposed that induction of the ERRA/ $\gamma$ signaling pathway can enhance mitochondrial function in both cell and animal models of mitochondrial disease. Our major findings include; 1) We recently compared in detail the different mitochondrial disease animal models (under review in Cell Metabolism). We found that the compound Ant1-/-ND6 mutant mouse model exhibited the earliest and strongest mitochondrial cardiomyopathy phenotype and therefore provided the best therapeutic window for our proposed intervention research strategy. 2) We discovered that GDF15 is a heart-derived hormone whose serum level correlates positively with the severity of mitochondrial cardiomyopathy (recently published with DOD grant support acknowledged), and it can be used as a biomarker in our studies.									
<b>15. SUBJECT TERMS</b> Mitochondria, mitochondrial disease, cardiomyopathy, estrogen-related receptor, transcriptional regulation, mitochondrial biogenesis, signaling, iPSCs, heart disease,									
<b>16. SECURITY CLASSIFICATION OF:</b>						<b>17. LIMITATION OF ABSTRACT</b>	<b>18. NUMBER OF PAGES</b>	<b>19a. NAME OF RESPONSIBLE PERSON</b>	
<b>a. REPORT</b>		<b>b. ABSTRACT</b>		<b>c. THIS PAGE</b>		Unclassified	38	USAMRMC	
Unclassified		Unclassified		Unclassified				<b>19b. TELEPHONE NUMBER</b> (include area code)	

## Table of Contents

	<u>Page</u>
<b>1. Introduction.....</b>	<b>1</b>
<b>2. Keywords.....</b>	<b>1</b>
<b>3. Accomplishments.....</b>	<b>1</b>
<b>4. Impact.....</b>	<b>8</b>
<b>5. Changes/Problems.....</b>	<b>9</b>
<b>6. Products.....</b>	<b>10</b>
<b>7. Participants &amp; Other Collaborating Organizations.....</b>	<b>12</b>
<b>8. Appendices.....</b>	<b>17</b>

- 1. INTRODUCTION:** We recently identified that two transcription factors, estrogen related receptor alpha (ERR $\alpha$ ) and gamma (ERR $\gamma$ ), are critical transcriptional regulators of mitochondrial biogenesis and function. Loss of both cardiac ERR $\alpha$  and ERR $\gamma$  in mice results in severe mitochondrial cardiomyopathy, heart failure and death within the first month of life. This is because that ERR $\alpha$  and ERR $\gamma$  are both sufficient and required to induce the transcription of many genes crucial for normal mitochondrial function and biogenesis. Overexpression of ERR $\alpha$  and ERR $\gamma$  increases mitochondrial biogenesis and function in cells. Therefore, we hypothesize that induction of the ERR $\alpha$ /ERR $\gamma$  signaling pathway (with both genetic and pharmacological approaches) can enhance mitochondrial function in both cells and tissues, thus providing a general approach for treating a broad spectrum of mitochondrial diseases. We propose to test our hypothesis using novel animal models of mitochondrial disease we recently developed.
- 2. KEYWORDS:** Mitochondria, mitochondrial disease, cardiomyopathy, estrogen related receptor, transcriptional regulation, mitochondrial biogenesis, signaling, iPSCs, heart disease

**3. ACCOMPLISHMENTS:**

- What were the major goals of the project?

Specific Aim 1 (specified in proposal)	Timeline	% complete
<b>Major Task 1</b>	<b>Months</b>	
Subtask 1: Treat mitochondrial cardiomyopathy in ND6 mutant mice	1-36	60%; <b>Wallace lab</b> has generated mice; <b>Pei lab</b> has generated virus
Subtask 2: Treat mitochondrial cardiomyopathy in CO1 mutant mice	1-36	60% <b>Wallace lab</b> has generated mice; <b>Pei lab</b> has generated virus
Milestone(s) Achieved: Successful completion of subtasks 1 and 2.	36	On track
IACUC Approval	1	100% August 09, 2016 <b>Wallace and Pei</b>
Milestone Achieved: HRPO/ACURO Approval	1	100% October 24, 2016 <b>Wallace and Pei</b>

<b>Specific Aim 2 (specified in proposal)</b>		
<b>Major Task 2</b>		
Subtask 1: Treat mitochondrial cardiomyopathy in Ant1-/- mice	1-36	60% <b>Wallace lab</b> has generated mice; <b>Pei lab</b> has generated virus
Milestone(s) Achieved: Successful completion of subtask 1.	36	On track
<b>Specific Aim 3 (specified in proposal)</b>		
<b>Major Task 3</b>		
Subtask 1: Improve mitochondrial and cellular functions in human Ant1-/- patient iPSCs-derived cardiomyocytes	13-36	50% <b>Pei lab</b>
Milestone(s) Achieved: Successful completion of subtask 1	36	On track

▪ **What was accomplished under these goals?**

1) Major activities: Overall we are on track to achieve our major research goals.

Aims 1 and 2: the **Wallace lab** recently published the detailed comparison of the different mitochondrial disease animal models ([Mitochondrial DNA Variation Dictates Expressivity and Progression of Nuclear DNA Mutations Causing Cardiomyopathy](#). McManus MJ, Picard M, Chen HW, De Haas HJ, Potluri P, Leipzig J, Towheed A, Angelin A, Sengupta P, Morrow RM, Kauffman BA, Vermulst M, Narula J, **Wallace** DC. Cell Metab. 2018 Aug 23. pii: S1550-4131(18)30503-5. PMID: 30174309 also see Appendices). Based on these latest results we decided to prioritize our research efforts on the compound Ant1-/-ND6 mutant mouse model, because this model exhibited the earliest and strongest mitochondrial cardiomyopathy phenotype and therefore provided the best therapeutic window for our proposed intervention research strategy. We devoted our efforts in this model in Year 1 and 2. The **Wallace lab** have maintained breeding colonies that have generated the several cohorts of compound Ant1-/-ND6 mutant mice for our experiments. The **Pei lab** has generated the AAV9-ERR $\gamma$  virus and the **Pei lab** has injected Ant1-/-ND6 mutant mice with AAV9-ERR $\gamma$  virus. We are currently measuring cardiac functions in these mice. We are also injecting more mice to reach to cohort number as we originally planned.

In order to determine the most reliable and earliest outcome measure for treatment, detailed analysis of the Ant1-/-ND6 mutant heart has been performed in mice between 1.5 and 9 months of age. Results from echocardiography are shown in Table 1 and Figure 1.

	ANT1-/- ND6						
	1.5 months old (n=4)	2 months old (n=4)	2.5 months old (n=4)	3 months old (n=4)	4 months old (n=3)	7.5 months old (n=4)	9 months old (n=5)
IVS;d (mm)	1.12 ± 0.06	1.00 ± 0.05	0.98 ± 0.04	1.05 ± 0.06	1.14 ± 0.09	1.27 ± 0.06	1.11 ± 0.11
IVS;s (mm)	1.60 ± 0.08	1.42 ± 0.06	1.42 ± 0.52	1.26 ± 0.10	1.17 ± 0.13	1.42 ± 0.12	1.31 ± 0.11
LVID;d (mm)	3.57 ± 0.04	4.00 ± 0.04	4.04 ± 0.13	4.25 ± 0.05	4.58 ± 0.18	4.57 ± 0.24	5.05 ± 0.25
LVID;s (mm)	2.23 ± 0.12	2.84 ± 0.11	2.79 ± 0.07	3.49 ± 0.09	3.90 ± 0.12	3.88 ± 0.20	4.53 ± 0.28
LVPW;d (mm)	0.94 ± 0.15	0.95 ± 0.06	0.88 ± 0.07	1.21 ± 0.15	0.90 ± 0.05	1.29 ± 0.13	1.15 ± 0.09
LVPW;s (mm)	1.35 ± 0.16	1.22 ± 0.03	1.18 ± 0.08	1.41 ± 0.06	1.04 ± 0.11	1.38 ± 0.13	1.23 ± 0.11
CO (LV Trace) (ml/min)	17.85 ± 1.29	18.66 ± 1.35	16.87 ± 1.06	17.02 ± 1.40	15.24 ± 1.44	14.76 ± 1.30	15.25 ± 2.39
EF (%)	67.75 ± 4.91	56.02 ± 4.29	59.01 ± 2.56	37.34 ± 3.02	31.49 ± 3.41	31.81 ± 1.21	22.55 ± 4.34
FS (%)	37.42 ± 3.98	29.05 ± 2.82	30.96 ± 1.82	17.87 ± 1.63	14.84 ± 1.79	14.96 ± 0.63	10.48 ± 2.13
LV Mass (mg)	140.65 ± 11.86	155.54 ± 11.37	145.82 ± 4.02	210.06 ± 14.70	206.88 ± 22.44	280.27 ± 16.17	277.92 ± 25.54
LV Mass (Corrected) (mg)	112.52 ± 9.46	124.44 ± 9.09	116.66 ± 3.22	168.05 ± 11.76	165.50 ± 17.95	224.22 ± 12.93	222.33 ± 20.43
LV Vol;d (mm)	53.24 ± 1.45	70.05 ± 1.48	72.19 ± 5.52	80.88 ± 2.06	96.86 ± 8.95	96.90 ± 12.24	122.84 ± 13.55
LV Vol;s (mm)	17.00 ± 2.23	30.76 ± 2.86	29.35 ± 1.89	50.72 ± 2.96	66.03 ± 5.08	66.07 ± 8.28	95.96 ± 14.12
SV (LV Trace) (ul)	39.54 ± 2.76	43.08 ± 3.41	42.50 ± 4.17	36.50 ± 3.96	33.10 ± 3.57	32.95 ± 3.10	33.66 ± 5.48

•Control:	Ctrl		
	2.5 months old (n=5)	3 months old (n=5)	4 months old (n=5)
IVS;d (mm)	0.8 ± 0.03	0.84 ± 0.07	0.92 ± 0.08
IVS;s (mm)	1.10 ± 0.05	1.29 ± 0.14	1.23 ± 0.09
LVID;d (mm)	4.27 ± 0.17	4.03 ± 0.06	4.34 ± 0.12
LVID;s (mm)	3.17 ± 0.17	2.56 ± 0.12	3.29 ± 0.10
LVPW;d (mm)	0.72 ± 0.10	0.76 ± 0.06	0.76 ± 0.03
LVPW;s (mm)	1.03 ± 0.09	1.17 ± 0.11	1.00 ± 0.07
CO (LV Trace) (ml/min)	15.61 ± 1.34	22.40 ± 3.13	20.36 ± 2.55
EF (%)	50.93 ± 3.13	66.30 ± 3.79	48.14 ± 1.70
FS (%)	25.83 ± 1.91	36.50 ± 2.97	24.07 ± 1.03
LV Mass (mg)	121.48 ± 7.32	120.81 ± 12.83	144.78 ± 12.94
LV Mass (Corrected) (mg)	97.18 ± 5.86	96.65 ± 10.27	115.83 ± 10.35
LV Vol;d (mm)	82.32 ± 7.66	71.48 ± 2.63	85.16 ± 5.71
LV Vol;s (mm)	40.77 ± 5.14	24.07 ± 2.85	44.22 ± 3.59
SV (LV Trace) (ul)	45.20 ± 2.82	50.33 ± 3.74	47.01 ± 4.34

Table 1. Echocardiography Results. A) Results from Ant1-/-ND6 mutant mice at given ages. B) Results from control mice (C57B6J) at given ages. IVS;d=interventricular septal end diastole, IVS;s=interventricular septal end systole, LVID;d=left ventricular internal diameter end diastole, LVID;s= left ventricular internal diameter end diastole, LVPW;d=Left ventricular posterior wall end diastole, LVPW;s=Left ventricular posterior wall end systole, CO=cardiac output, EF=ejection fraction, FS=fraction shortening, LV Vol;d= left ventricular volume diastolic, , LV Vol;s= left ventricular volume systolic, SV= Stroke volume

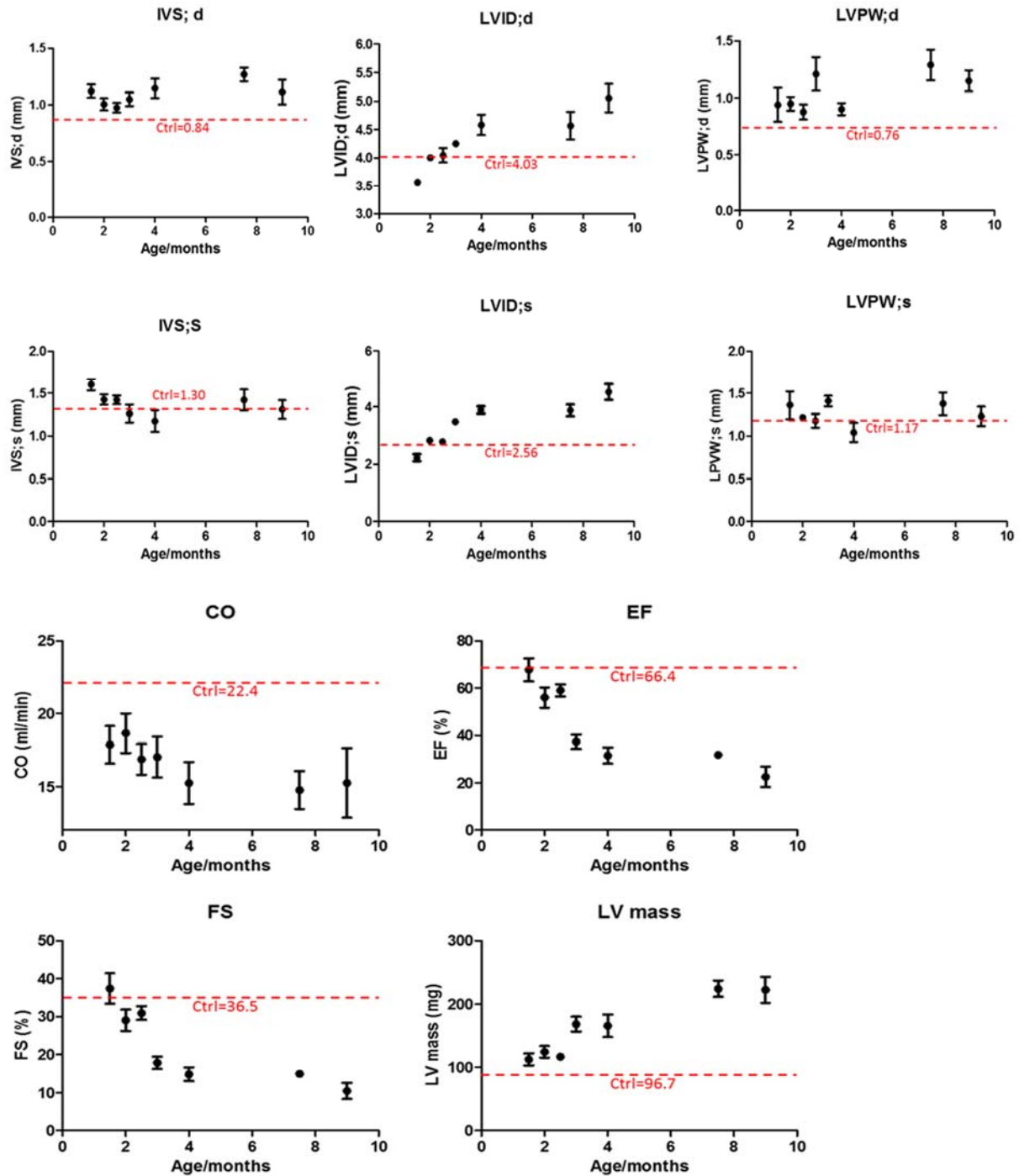


Figure 1. Echocardiography of Ant1-/-ND6 mutant mice. IVS;d=interventricular septal end diastole, IVS;s=interventricular septal end systole, LVID;d=left ventricular internal diameter end diastole, LVID;s= left ventricular internal diameter end diastole, LVPW;d=Left ventricular posterior wall end diastole, LVPW;s=Left ventricular posterior wall end systole, CO=cardiac output, EF=ejection fraction, FS=fraction shortening, LV Vol;d= left ventricular volume diastolic, LV Vol;s= left ventricular volume systolic, SV= Stroke volume

These experiments demonstrate that the Ant1<sup>-/-</sup>ND6 mutants present with cardiac changes by three months of age. These results have informed the therapeutic experiments, and the Pei lab is now injecting AAV9-ERR $\gamma$  into control and Ant1<sup>-/-</sup>ND6 mutant mice at 2 time points: 1 month of age via ultrasound-assisted injection, and 3 days of age via direct pericardial injection. We expect to complete all studies in Aim 1 and 2 by end of Year 3.

Aim 3: **Pei lab** has initiated studies in Aim 3 using Ant1<sup>-/-</sup> iPSC-derived cardiomyocytes. We have measured and evaluated mitochondrial functions in control and ERR $\gamma$  overexpressed cardiomyocytes. Our initial results show that ERR $\gamma$  increases mitochondrial membrane potential (Figure 2) and calcium signaling (Figure 3), supporting our hypothesis that ERR $\gamma$  may increase mitochondrial functions in Ant1<sup>-/-</sup> cells. We are currently completing experiments to measure other aspects of mitochondrial functions (respiration, morphology, etc) as we originally proposed. We expect to complete all studies in Aim 3 by end of Year 3.

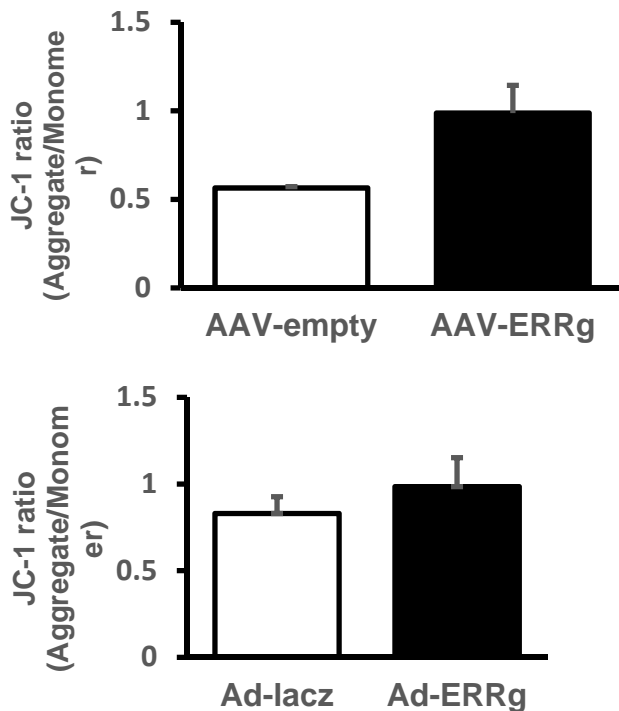


Figure 2. Membrane potential in Ant1<sup>-/-</sup> iPSCs transduced with AAV9-ERR $\gamma$ . Membrane potential in Ant1<sup>-/-</sup> iPSCs was measured using JC-1 dye.

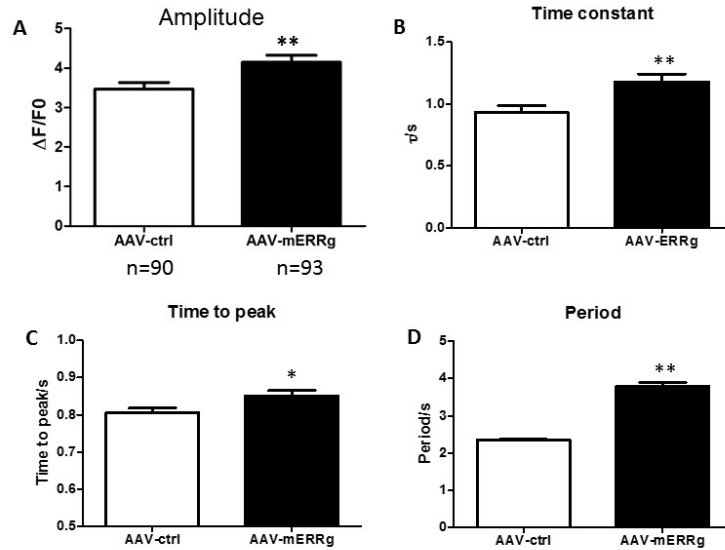


Figure 3. Calcium transients measured in Ant1<sup>-/-</sup> iPSCs transduced with AAV9-ERR $\gamma$ . (A) fluorescence normalized to baseline. (B) time constant. (C) time to peak. (D) period. F: fluorescence; Fo: baseline fluorescence

- 2) Specific objectives: In addition to aforementioned progress in major activities, **Pei and Wallace** together have successfully achieved milestones of institute IACUC protocol and ACURO approvals on time.
- 3) Significant results and key outcomes:
  - o **Pei lab** has previously discovered that GDF15 is a heart-derived hormone that regulates body growth. Circulating GDF15 level correlates positively with the severity of mitochondrial cardiomyopathy and can be used as a serum biomarker for our mitochondrial disease studies. **Pei lab** has further identified the molecular mechanism of GDF15 upregulation in mitochondrial cardiomyopathy. This work was just published (see appendices) and the DOD grant support was acknowledged. We will take advantage of these new findings and monitor serum GDF15 level as an additional, more convenient and less invasive method to determine whether mitochondrial cardiomyopathy was ameliorated by ERR $\gamma$  overexpression and activation (Aims 1 and 2). **Pei lab** has also published a paper discovering that ERR $\gamma$  is important to maintain mitochondrial functions in the kidney, another organ often affected in mitochondrial disease (see appendices).
  - o **Wallace lab** recently published results of the different mitochondrial disease animal models (see Appendices). We found that the compound Ant1<sup>-/-</sup>ND6 mutant mouse model exhibited the earliest and strongest mitochondrial cardiomyopathy phenotype and therefore provided the best therapeutic window for our proposed intervention research strategy.

4) Other accomplishments: Our recent publications in Year 2 that are supported by this DOD grant are attached in the appendices.

▪ **What opportunities for training and professional development has the project provided?**

- Training: Dr. Zhao has received one-on-one training in iPSC technology, gene editing and single cell or nucleus RNA-Seq.
- Professional Development: Dr. **Pei** attended the United Mitochondrial Disease Foundation annual meeting in Nashville, June 27-30, 2018. He met with many fellow researcher in mitochondrial disease. He also met many mitochondrial disease patients and family members and learned more about their life. He is eager to continue to contribute to our cause to cure mitochondrial disease one day.

▪ How were the results disseminated to communities of interest?

First, the Pei and Wallace labs have published series of papers on or related to ERR $\gamma$  and mitochondrial functions:

- The **Pei lab** has published several papers:
  - ❖ Zhao J, Lupino K, Wilkins BJ, Qiu C, Liu J, Omura Y, Allred AL, McDonald C, Susztak K, Barish GD, **Pei L.** (2018) Genomic integration of ERR $\gamma$ -HNF1 $\beta$  regulates renal bioenergetics and prevents chronic kidney disease. *Proceedings of National Academy of Sciences* 115, E4910-E4919. PMID: 29735694.
  - ❖ Li J, Liu J, Lupino K, Liu X, Zhang L, **Pei L.** (2018) GDF15 maturation requires proteolytic cleavage by PCSK3, 5 and 6. *Molecular and Cellular Biology*. PMID: 30104250.
  - ❖ Hu P, Liu J, Zhao J, Wilkins BJ, Lupino K, Wu H, **Pei L.** (2018). Single-nucleus transcriptomic survey of cell diversity and functional remodeling in the postnatal developing hearts. *Genes & development* 32, 1344-1357. PMID: 30254108.
- The **Wallace lab** has published a manuscript in *Cell Metabolism* that described the cardiac phenotype of mice with combined mutations in mitochondrial and nuclear genes.
  - ❖ Mitochondrial DNA Variation Dictates Expressivity and Progression of Nuclear DNA Mutations Causing Cardiomyopathy. McManus MJ, Picard M, Chen HW, De Haas HJ, Potluri P, Leipzig J, Towheed A, Angelin A, Sengupta P, Morrow RM, Kauffman BA, Vermulst M, Narula J, **Wallace DC.** *Cell Metab.* 2018 Aug 23. pii: S1550-4131(18)30503-5. PMID:30174309

- Drs. **Pei and Wallace** together published a review of mitochondria and disease:
  - ❖ **Pei L, Wallace DC** (2018). Mitochondrial Etiology of Neuropsychiatric Disorders. Biological psychiatry 83, 722-730. PMID: 29290371. PMCID: PMC5891364

In addition, Drs. **Pei and Wallace** have been invited to give talks in numerous national/international meetings and in academic institutions about their work on this topic (please see below in “6. PRODUCTS)

- What do you plan to do during the next reporting period to accomplish the goals?

We plan to finish all proposed goals and experiments in all research aims. For Aims 1 and 2, the Pei lab will complete injecting AAV9-ERR $\gamma$  to all Ant1-/-ND6 mutant mice as planned, and the Pei lab will measure their cardiac functions periodically to determine whether overexpression of ERR $\gamma$  improves cardiac function in these mice. For Aim 3 the Pei and Wallace labs will complete studies to determine whether ERR $\gamma$  overexpression has improved mitochondrial functions in Ant1-/- iPSC-differentiated cardiomyocytes.

#### **4. IMPACT:**

- What was the impact on the development of the principal discipline(s) of the project?

The **Pei lab** has recently discovered that GDF15 is a heart-derived hormone that regulates body growth. Circulating GDF15 level correlates positively with the severity of mitochondrial cardiomyopathy and can be used as a serum biomarker for our mitochondrial disease studies.

The **Pei lab** has further identified the molecular mechanism of GDF15 upregulation in mitochondrial cardiomyopathy. This work was just published (see appendices) and the DOD grant support was acknowledged. We will take advantage of these new findings and monitor serum GDF15 level as an additional, more convenient and less invasive method to determine whether mitochondrial cardiomyopathy was ameliorated by ERR $\gamma$  overexpression and activation (Aims 1 and 2). **Pei lab** has also published a paper discovering that ERR $\gamma$  is important to maintain mitochondrial functions in the kidney, another organ often affected in mitochondrial disease (see appendices).

- **What was the impact on other disciplines?**

The **Pei lab** recently discovered that GDF15 is a heart-derived hormone that regulates body growth. Pediatric heart disease induces GDF15 synthesis and secretion by cardiomyocytes. Circulating GDF15 in turn acts on the liver to inhibit growth hormone (GH) signaling and body growth. We demonstrate that blocking cardiomyocyte production of GDF15 normalizes circulating GDF15 level and restores liver GH signaling, establishing GDF15 as a bona fide

heart-derived hormone that regulates pediatric body growth. Importantly, plasma GDF15 is further increased in children with concomitant heart disease and failure to thrive (FTT). Together these studies reveal a new endocrine mechanism by which the heart coordinates cardiac function and body growth. Our results also provide a potential mechanism for the well-established clinical observation that children with heart diseases often develop FTT. The **Pei lab** has further identified the molecular mechanism of GDF15 upregulation in mitochondrial cardiomyopathy. This work was just published (see appendices) and the DOD grant support was acknowledged. We will take advantage of these new findings and monitor serum GDF15 level as an additional, more convenient and less invasive method to determine whether mitochondrial cardiomyopathy was ameliorated by  $ERR\gamma$  overexpression and activation (Aims 1 and 2). The **Pei lab** has also published a paper discovering that  $ERR\gamma$  is important to maintain mitochondrial functions in the kidney, another organ often affected in mitochondrial disease (see appendices).

- **What was the impact on technology transfer?**

Nothing to Report

- **What was the impact on society beyond science and technology?**

Johnson & Johnson named Douglas Wallace, Ph.D. winner of the 2017 Dr. Paul Janssen Award for Biomedical Research, and launched a campaign for champions of science as part of the Dr. Paul Janssen Project – a new year-long, multi-faceted program to recognize the impact of science on humanity. Dr. Wallace won for his pioneering work in the field of mitochondrial genetics, and joined 14 other scientists who have received the Dr. Paul Janssen Award in the past 13 years, including two who went on to win the Nobel Prize. The ceremony included a talk by Dr. Wallace on the importance of the mitochondria in health and disease.

## **5. CHANGES/PROBLEMS:**

- **Changes in approach and reasons for change**

As detailed above, we have prioritized the compound Ant1-/-ND6 mutant mouse model based on our latest research results. This model exhibited the earliest and strongest mitochondrial cardiomyopathy phenotype and therefore provided the best therapeutic window for our proposed intervention research strategy. We devoted our efforts in this model in Year 2 and moving forward. We also prioritized AAV9 to deliver  $ERR\gamma$  using two different approaches

(ultrasound guided injection in adult mice, or pericardial injection in newborn mice) against the pharmacological activation of ERR $\gamma$  as we are still determining the optimal dose.

- **Changes that had a significant impact on expenditures**

Nothing to report

- **Significant changes in use or care of human subjects, vertebrate animals, biohazards, and/or select agents**

Nothing to report

- **Significant changes in use or care of human subjects**

Nothing to report

- **Significant changes in use or care of vertebrate animals.**

Nothing to report

- **Significant changes in use of biohazards and/or select agents**

Nothing to report

## 6. PRODUCTS:

- **Publications, conference papers, and presentations**

- **Journal publications.**

The **Pei lab** has published several papers:

- ❖ Zhao J, Lupino K, Wilkins BJ, Qiu C, Liu J, Omura Y, Allred AL, McDonald C, Susztak K, Barish GD, **Pei L.** (2018) Genomic integration of ERR $\gamma$ -HNF1 $\beta$  regulates renal bioenergetics and prevents chronic kidney disease. *Proceedings of National Academy of Sciences* 115, E4910-E4919. PMID: 29735694.
- ❖ Li J, Liu J, Lupino K, Liu X, Zhang L, **Pei L.** (2018) GDF15 maturation requires proteolytic cleavage by PCSK3, 5 and 6. *Molecular and Cellular Biology*. PMID: 30104250.
- ❖ Hu P, Liu J, Zhao J, Wilkins BJ, Lupino K, Wu H, **Pei L.** (2018). Single-nucleus transcriptomic survey of cell diversity and functional remodeling in the postnatal developing hearts. *Genes & development* 32, 1344-1357. PMID: 30254108.

The **Wallace lab** has published a manuscript in *Cell Metabolism* that described the cardiac phenotype of mice with combined mutations in mitochondrial and nuclear genes.

- ❖ Mitochondrial DNA Variation Dictates Expressivity and Progression of Nuclear DNA Mutations Causing Cardiomyopathy. McManus MJ, Picard M, Chen HW, De Haas HJ,

Potluri P, Leipzig J, Towheed A, Angelin A, Sengupta P, Morrow RM, Kauffman BA, Vermulst M, Narula J, **Wallace DC**. Cell Metab. 2018 Aug 23. pii: S1550-4131(18)30503-5. PMID:30174309

Drs. **Pei and Wallace** together published a review of mitochondria and disease:

❖ **Pei L, Wallace DC** (2018). Mitochondrial Etiology of Neuropsychiatric Disorders. Biological psychiatry 83, 722-730. PMID: 29290371. PMCID: PMC5891364

▪ **Books or other non-periodical, one-time publications.**

Nothing to report

▪ **Other publications, conference papers, and presentations.**

○ **Liming Pei presentations**

- ❖ 09/2017, Inaugural Canadian Mitochondrial Disease Conference, Toronto, Canada. “A heart-derived hormone that connects failure to thrive to mitochondrial disease”
- ❖ 10/2017, Institute for Diabetes and Obesity (IDO), Helmholtz Zentrum München, Munich, Germany, “Listen to your heart – a heart-derived hormone that regulates body growth”
- ❖ 01/2018, Department of Biochemistry & Molecular Medicine, University of California, Davis. Sacramento, CA. “Listen to your heart – a heart-derived hormone that regulates body growth”
- ❖ 06/2018, Center for Pharmacogenetics, Department of Pharmaceutical sciences, University of Pittsburgh, Pittsburgh, PA. “Listen to your heart – a heart-derived hormone that regulates body growth”
- ❖ 06/2018, Gordon Research Conference – Cardiac Regulatory Mechanism, New London, NH. “Single-nucleus transcriptomic survey of cell diversity and functional maturation in the postnatal mammalian hearts”
- ❖ 08/2018, Department of Molecular Biology, UT Southwestern Medical Center, Dallas, TX. “Cardiac endocrinology – heart-derived hormones in physiology and disease”
- ❖ 09/2018, Molecular Metabolism Seminar Series, David Geffen School of Medicine at UCLA, Los Angeles, CA. “Cardiac endocrinology – heart-derived hormones in physiology and disease”
- ❖ 09/2018, Department of Medicine, Northwestern University, Chicago, IL. “Listen to your heart – a heart-derived hormone that regulates body growth”

**Doug Wallace presentations**

- ❖ Sept, 2017 “Mitochondrial DNA Variation in Human Evolution and Disease”, Mitochondrial Evolutionary Genomics Conference Keynote Speaker, Ein Gedi, Israel
- ❖ Sep, 2017 “The Mitochondrion: Our Origins – Our Diseases”, 2017 Dr. Paul Janssen Award Symposium, New York City, NY
- ❖ Sep, 2017 “A Mitochondrial Etiology of Metabolic and Degenerative Diseases”, The Canada Mitochondrial Network and MitoCanada Foundation, Toronto, Canada
- ❖ Oct, 2017 “The Mitochondrion: Our Origins – Our Diseases”, Genetics and Complex Diseases, Harvard Chan School, Boston, MA
- ❖ Oct, 2017 “A Mitochondrial Etiology of Complex Diseases”, University of Pennsylvania Perelman School of Medicine, Department of Cardiovascular Institute Seminar Series, Philadelphia, PA
- ❖ Oct, 2017 “Mitochondria: Our Origins-Our Diseases”, Cornell University, Ithaca, NY
- ❖ Oct, 2017 “Our Origins-Our Diseases: The Mitochondrial Perspective”, Golden Sages Lecture, Bryn Mawr College, Bryn, Mawr, PA
- ❖ Oct, 2017 “A Mitochondrial Etiology of Complex Diseases and Associated Inflammation”, University of Pennsylvania Perelman School of Medicine, Penn Transplant Institute Research Lecture, Philadelphia, PA
- ❖ Oct, 2017 “Mitochondria: Our Origins-Our Diseases”, the 12<sup>th</sup> Annual International Conference in Genomics, Shenzhen, China
- ❖ Nov, 2017 “Mitochondrial Variation in Metabolic and Degenerative Diseases, Cancer, & Aging”, University of Chicago Cancer Biology Seminar Series, Chicago, IL
- ❖ Nov, 2017 “Mitochondrial Genetic Variation in Human Evolution and Disease”, Cleveland Clinic, Cleveland, OH
- ❖ Dec, 2017 “Mitochondrial Genetics and Disease Risk: What Is the Current Evidence?”, Nutrigenomics and the Future of Nutrition-Food Forum Meeting at the National Academy of Sciences, Washington, DC
- ❖ Jan, 2018 “A Mitochondrion Etiology of the Common “Complex” Diseases”, Rutgers Cancer Center, New Brunswick, NJ
- ❖ Jan, 2018 “A Mitochondrial Etiology of Neuroophthalmological Diseases”, Basic Science Course in Ophthalmology at Columbia University
- ❖ Jan, 2018 “A Mitochondrion Etiology of the Common “Complex” Diseases”, 2018 Inaugural Mitochondrial Medicine Distinguished Lecture at Columbia University
- ❖ Feb, 2018 “A Mitochondrial Etiology Of The Common ‘Complex’ Diseases”, University of California San Diego at the Rady Children’s Hospital of San Diego, San Diego, CA
- ❖ March, 2018 “The Enigma of Traditional Eastern Medicine”, Bench to Bedside Research Symposium, University of California, Irvine Medical School, Irvine, CA
- ❖ April, 2018 “Why Can’t We Understand and Cure the Common Diseases? An Energyomics Perspective”, Keynote Speaker at the American Council of Life Insurers Genetics Symposium (ACLI), Washington, DC
- ❖ April, 2018 “Mitochondrial Genetic Variation in Human Evolution and Disease”, the First AsiaEvo Conference, Shenzhen, China
- ❖ April, 2018 “Mitochondria from Evolution to Disease: It’s in the Genes”, the 2018 AUA-IARS Joint Symposium: Mitochondria and Bioenergetics in Health and

- ❖ Disease: It's Not Just a Power Failure, Chicago, IL
- ❖ May, 2018 "Mitochondrial Etiology of Common Diseases", the University of Arkansas Seminar, Fayetteville, AR
- ❖ May, 2018 "Mitochondrial in the Etiology of Traumatic, Acute, and Chronic Disease", the Center for Injury Research and Prevention Guest Lecture at Children's Hospital of Philadelphia, Philadelphia, PA
- ❖ May, 2018 "Mitochondrial biology in disease and modern medicine", the American Thoracic Society International Conference, San Diego, CA
- ❖ May, 2018 "A Mitochondrial Etiology of Common "Complex" Diseases", the International Conference on Subcellular Organelles 2018 at the Shanghai International Convention Center, Shanghai, China
- ❖ May, 2018 "A Mitochondrial Etiology of Common Disease", Institute of Genetics Zhejiang University, Huanzhou, China.
- ❖ June, 2018 "Mitochondrial Biophysics and the Etiology of Disease", Britten Chance Symposium, U. Pennsylvania
- ❖ June, 2018 "A Mitochondrial Etiology of Common Diseases", Marsh Lecture in Molecular Medicine, Feinstein Institute of Biomedical Research, Northwell Hospital System, Manhasset, NY.
- ❖ June, 2018 "A Mitochondrial Etiology of Common Diseases" 2018 International Symposium in Biomedical Sciences, China Medical University, Taichung, Taiwan.
- ❖ June, 2018 "Clinical Implication of Mitochondrial Medicine" Changhua Christian Hospital, Taichung, Taiwan.
- ❖ July, 2018 "Clinical Implication of Mitochondrial Medicine" 60th Anniversary Celebration of the Department of Genetics, Stanford University, Palo Alto, CA.
- ❖ August, 2018 "A Mitochondrial Etiology of Cardiovascular Disease", "Clinical Implication of Mitochondrial Medicine", NHLBI, Bethesda, MD
- ❖ August, 2018 "A mitochondrial Etiology of Common Diseases", 20th European Bioenergetics Conference (EBEC2018), Budapest, Hungary.

○

- **Website(s) or other Internet site(s)**

[www.mitomap.org](http://www.mitomap.org). MITOMAP reports published and unpublished data on human mitochondrial DNA variation. Currently our variant tables report frequencies from 30589 human mitochondrial DNA sequences.

- **Technologies or techniques**

nothing to report

- **Inventions, patent applications, and/or licenses**

nothing to report

- **Other Products**

nothing to report

## 7. PARTICIPANTS & OTHER COLLABORATING ORGANIZATIONS

- What individuals have worked on the project?

Name:	<i>Douglas C. Wallace, Ph.D.</i>
Project Role:	<i>No change</i>
Name:	<i>Liming Pei, Ph.D.</i>
Project Role:	<i>No change</i>
Name:	<i>Deborah G. Murdock, Ph.D.</i>
Project Role:	<i>No change</i>
Name:	<i>Jesus Tintos Hernandez, Ph.D.</i>
Project Role:	<i>Postdoctoral fellow</i>
Nearest person month worked:	<i>3</i>
Contribution to Project:	<i>Dr. Hernandez has been instrumental in creation and maintenance of iPSCs</i>
Name:	<i>Juanjuan Zhao, Ph.D.</i>
Project Role:	<i>Postdoctoral fellow</i>
Nearest person month worked:	<i>12</i>
Contribution to Project:	<i>Dr Zhao has been responsible for designing and producing AAV9-ERR viruses and evaluating cardiac function both in animal (Aims 1 and 2) and cell (Aim 3) models of mitochondrial disease.</i>
Funding Support:	
Name:	<i>Katherine Lupino</i>
Project Role:	<i>Research technician</i>

Nearest person month worked:	10
Contribution to Project:	<i>Miss Lupino has provided technical support in maintain mouse colonies and cell cultures. Miss Lupino replaced Caitlin McDonald</i>
Funding Support:	
Name:	<i>Arrienne Butic</i>
Project Role:	<i>Research technician</i>
Nearest person month worked:	1
Contribution to Project:	<i>Ms Butic has replaced D Rittenhouse as the research technician responsible for mouse husbandry.</i>
Funding Support:	
Name:	<i>Jian Liu</i>
Project Role:	<i>Postdoctoral fellow</i>
Nearest person month worked:	1
Contribution to Project:	<i>Dr. Jian Liu has been responsible for working with and assisting Dr. Juanjuan Zhao in designing and producing AAV9-ERR<math>\gamma</math> viruses and evaluate cardiac function both in animal (Aims 1 and 2) and cell (Aim 3) models of mitochondrial disease.</i>

- **Has there been a change in the active other support of the PD/PI(s) or senior/key personnel since the last reporting period?**

No changes for other active research support for Dr. Liming Pei

Changes for other active research support for Dr. Douglas are:

❖ 5R01-NS021328-30 (PI D. Wallace) 04/01/13 – 03/31/18 1.2 calendar months  
National Institutes of Health (NIH) \$261,528

***Mitochondrial Inborn Errors of Metabolism***

This project will investigate the genetics of maternally inherited neurological diseases.

**Role:** PI

There is no scientific or budgetary overlap. **This grant has ended since the last reporting period.**

❖ 100041003 (PI D. Wallace) 10/01/14 – 12/31/17 0.24 calendar months  
GlaxoSmithKline \$119,048

***Mitochondria and Chronic Obstructive Pulmonary Disease: A LHON Connection***

This project will investigate how mtDNA cybrids can be used to test the efficacy of increasing antioxidant defenses by activation of Nrf2 or reducing mtDNA oxidative damage by over expression of OGG1.

**Role:** PI

There is no scientific or budgetary overlap. **This grant has ended since the last reporting period.**

❖ N/A (PI Atif Towheed/D. Wallace) 07/01/15 – 07/31/18 1.2 calendar months  
United Mitochondrial Disease Foundation \$35,000

***Allotopic RNA Rescue of LHON Mouse Models***

This project will investigate the use of a novel gene therapy approach in correcting the mutant phenotype in a LHON mouse model

**Role:** Fellowship Grant

There is no scientific or budgetary overlap. **This grant has been extended**

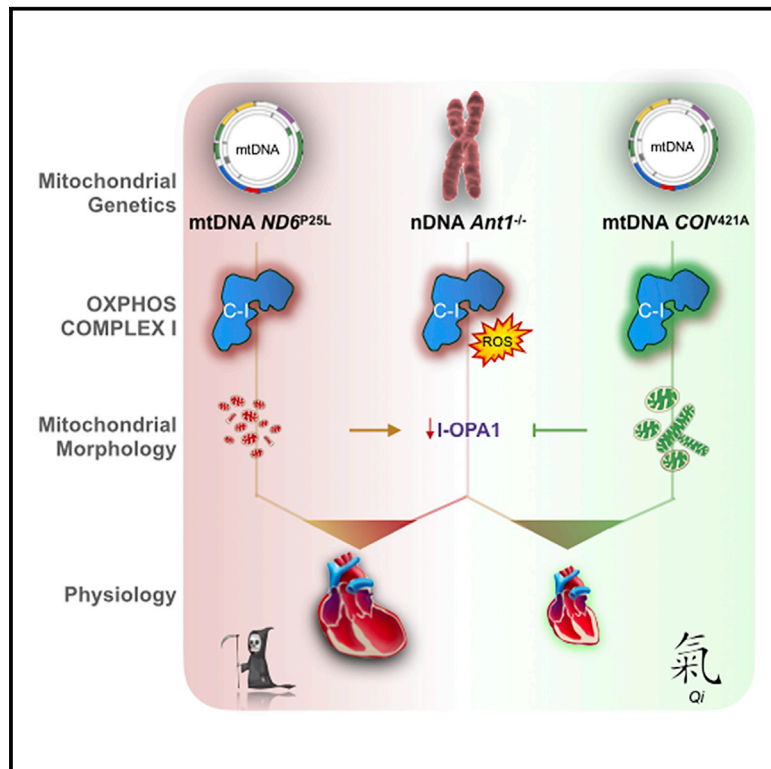
▪ **What other organizations were involved as partners?**

Nothing to Report

# Cell Metabolism

## Mitochondrial DNA Variation Dictates Expressivity and Progression of Nuclear DNA Mutations Causing Cardiomyopathy

### Graphical Abstract



### Authors

Meagan J. McManus, Martin Picard, Hsiao-Wen Chen, ..., Marc Vermulst, Jagat Narula, Douglas C. Wallace

### Correspondence

wallaced1@email.chop.edu

### In Brief

McManus et al. investigate mitochondrial-nuclear interactions in human disease by developing a murine model combining the *Slc25a4* cardiomyopathy null gene mutation with mild mtDNA variants. Differences in mtDNA genotype can strongly influence autosomal gene mutations; conversely, accumulation of somatic mtDNA mutations can augment the deleterious consequences of mitochondrial-nuclear interactions.

### Highlights

- Mitochondrial-nuclear interactions modulate autosomal mutation expressivity
- mtDNA complex I and IV variants have opposing effects on *Ant1*<sup>-/-</sup> pathophysiology
- *Ant1*<sup>-/-</sup> decreases OXPHOS complex I amount and complex V structural assembly
- Somatic mtDNA mutations augment the effects of unfavorable mtDNA-nDNA interactions

# Mitochondrial DNA Variation Dictates Expressivity and Progression of Nuclear DNA Mutations Causing Cardiomyopathy

Meagan J. McManus,<sup>1</sup> Martin Picard,<sup>1,2</sup> Hsiao-Wen Chen,<sup>1</sup> Hans J. De Haas,<sup>3</sup> Prasanth Potluri,<sup>1</sup> Jeremy Leipzig,<sup>1</sup> Atif Towheed,<sup>1</sup> Alessia Angelin,<sup>1</sup> Partho Sengupta,<sup>3,6</sup> Ryan M. Morrow,<sup>1</sup> Brett A. Kauffman,<sup>4</sup> Marc Vermulst,<sup>1</sup> Jagat Narula,<sup>3</sup> and Douglas C. Wallace<sup>1,5,7,\*</sup>

<sup>1</sup>Center for Mitochondrial and Epigenomic Medicine, The Children's Hospital of Philadelphia and University of Pennsylvania, Colket Translational Research Building, Room 6060, 3501 Civic Center Boulevard, Philadelphia, PA 19104-4302, USA

<sup>2</sup>Departments of Psychiatry and Neurology, Columbia University Medical Center, New York, NY 10032, USA

<sup>3</sup>Department of Medicine, Mount Sinai Hospital, New York, NY 10029, USA

<sup>4</sup>Vascular Medicine Institute, University of Pittsburgh, Pittsburgh, PA 15261, USA

<sup>5</sup>Department of Pathology and Laboratory Medicine, University of Pennsylvania, Philadelphia, PA 19104, USA

<sup>6</sup>Present address: Division of Cardiology, WVU Heart & Vascular Institute, West Virginia University School of Medicine, Morgantown, WV 26506-8059, USA

<sup>7</sup>Lead Contact

\*Correspondence: [wallaced1@email.chop.edu](mailto:wallaced1@email.chop.edu)

<https://doi.org/10.1016/j.cmet.2018.08.002>

## SUMMARY

Nuclear-encoded mutations causing metabolic and degenerative diseases have highly variable expressivity. Patients sharing the homozygous mutation (c.523delC) in the adenine nucleotide translocator 1 gene (*SLC25A4*, *ANT1*) develop cardiomyopathy that varies from slowly progressive to fulminant. This variability correlates with the mitochondrial DNA (mtDNA) lineage. To confirm that mtDNA variants can modulate the expressivity of nuclear DNA (nDNA)-encoded diseases, we combined in mice the nDNA *Slc25a4*<sup>-/-</sup> null mutation with a homoplasmic mtDNA *ND6*<sup>P25L</sup> or *COI*<sup>V421A</sup> variant. The *ND6*<sup>P25L</sup> variant significantly increased the severity of cardiomyopathy while the *COI*<sup>V421A</sup> variant was phenotypically neutral. The adverse *Slc25a4*<sup>-/-</sup> and *ND6*<sup>P25L</sup> combination was associated with impaired mitochondrial complex I activity, increased oxidative damage, decreased I-OPA1, altered mitochondrial morphology, sensitization of the mitochondrial permeability transition pore, augmented somatic mtDNA mutation levels, and shortened lifespan. The strikingly different phenotypic effects of these mild mtDNA variants demonstrate that mtDNA can be an important modulator of autosomal disease.

## INTRODUCTION

Mitochondrial dysfunction may play a critical role in the pathophysiology of complex metabolic and degenerative diseases (Wallace, 2013b). One such disease is cardiomyopathy, in which mitochondrial dysfunction has been demonstrated in both pedi-

atric and adult cases (Murphy et al., 2016; Porter et al., 2011; Zaragoza et al., 2011).

The mitochondrial proteome is encoded by 1,000 to 2,000 nDNA genes and by hundreds to thousands of copies of the maternally inherited mtDNA. The mtDNA encodes for 13 essential polypeptides required for energy production via oxidative phosphorylation (OXPHOS). The energetically favorable transfer of electrons through OXPHOS complexes I–IV is used to generate an electrochemical gradient across the mitochondrial inner membrane that is utilized by complex V (H<sup>+</sup>-pumping F<sub>1</sub>F<sub>0</sub>-ATP synthase) to produce ATP. Mitochondrial matrix ATP is then exchanged for cytosolic ADP by the inner membrane adenine nucleotide translocators (ANTs). In addition to ATP/ADP translocation, the ANTs regulate the mitochondrial permeability transition pore (mtPTP) in distinct ways depending upon the isoform (Bauer et al., 1999; Chevrollier et al., 2011; Jang et al., 2008; Kokoszka et al., 2004; Zamora et al., 2004a, 2004b). Humans have four ANT isoforms, while mice have three, but both species express the heart-muscle-brain isoform, ANT1 (*SLC25A4*), and the systemic isoform, ANT2 (*SLC25A5*), in the heart (Kokoszka et al., 2016). Hence, inactivation of the *SLC25A4* gene will result in a partial cardiac ANT defect.

Inactivating mutations in *ANT1* cause autosomal recessive myopathy and cardiomyopathy (Echaniz-Laguna et al., 2012; Palmieri et al., 2005). However, the severity of ANT1-deficient cardiomyopathy can be variable, and this variability has been correlated with the mtDNA lineage (Strauss et al., 2013).

There are three types of clinically relevant mtDNA variations: functional polymorphisms, which are associated with ancient mtDNA lineages called haplogroups, recent deleterious mutations that can result in maternally inherited disease, and somatic mutations that accumulate in tissues over time. The phenotypic consequences of these different types of mtDNA variation are interdependent (Ji et al., 2012) and may be modulated by interactions with nDNA variants, as well as the environment (Wallace, 2013a). Due to these complex interactions, the etiological significance of mtDNA variation in common, age-related diseases has

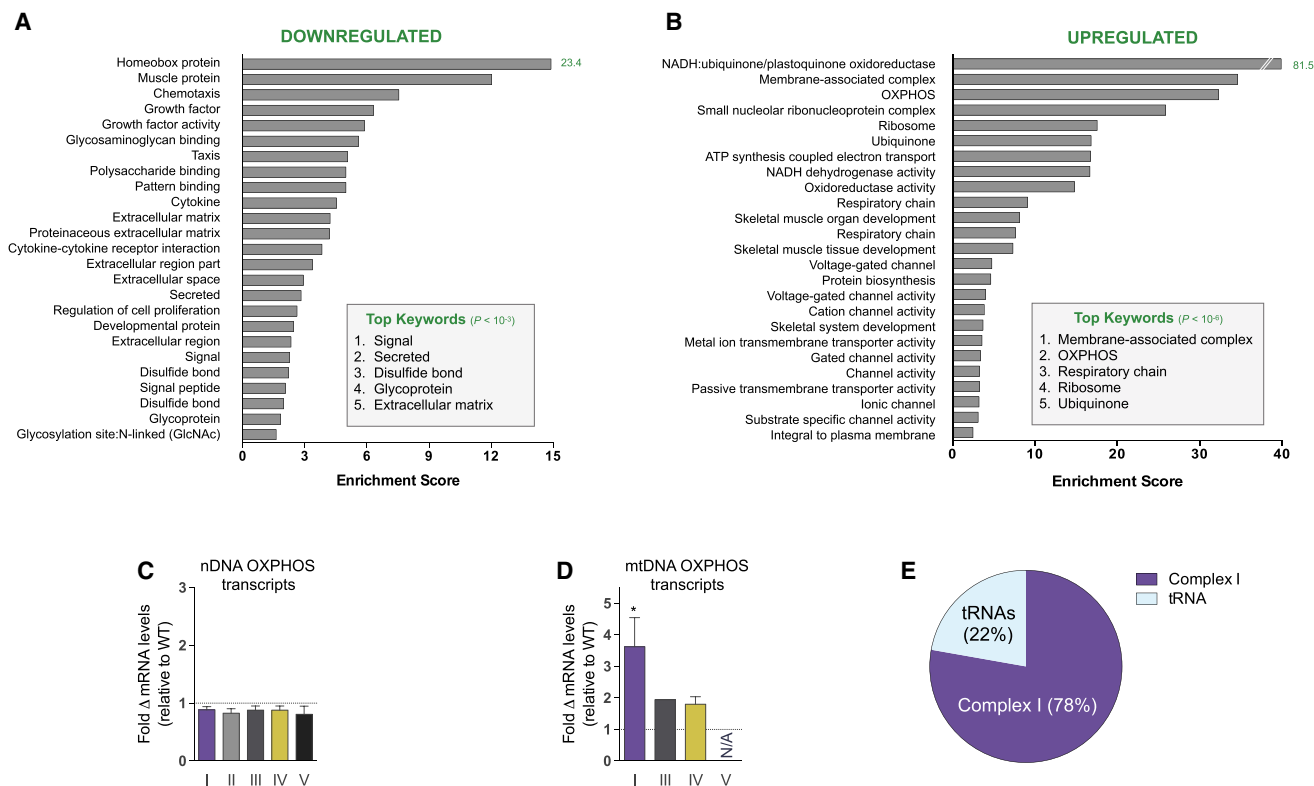


**Figure 1. ANT1-Deficiency Induces Transcriptional Changes Associated with Pathological Remodeling of the Heart**

(A and B) Twenty-five most significantly downregulated ( $>2$ -fold, total = 459; A) and upregulated ( $<0.4$ -fold, total = 363; B) functionally annotated gene categories in *Ant1*-null myocardium compared with WT. Searched categories include Gene Ontology, Protein Information Resource, Sequence (Seq) Features, Kyoto Encyclopedia of Genes and Genomes, InterPro protein sequence, and analysis classification. Analysis performed using the Database for Annotation, Visualization and Integrated Discovery (DAVID, v6.7).

(C and D) (C) Fold change in mRNA transcripts from nDNA and (D) mtDNA OXPHOS genes by complex relative to WT ( $*p < 0.05$ ).

(E) Portion of differentially expressed RNA transcripts from mtDNA.  $n = 4$ .

See also Figure S1 and Table S1.

been difficult to delineate (Zaragoza et al., 2011). Therefore, the significance of mtDNA contribution to cardiomyopathy in which patients harbor mtDNA variants along with nDNA contractile protein mutations (Arbustini et al., 1998a, 1998b) or *Ant1* mutations (Strauss et al., 2013) remains to be clarified.

To address this knowledge gap, we have developed a mouse model of mitochondrial cardiomyopathy by combining the *Slc25a4* (*Ant1*) null gene mutation (Graham et al., 1997; Narula et al., 2011) with two different mild mtDNA variants. These mtDNA variants are the NADH dehydrogenase subunit 6 (*ND6*) gene nucleotide 13997G>A missense mutation (*ND6*<sup>P25L</sup>) causing a partial complex I defect (Lin et al., 2012) and the cytochrome *c* oxidase subunit 1 gene (*COI*) nucleotide 6589T>C missense mutation (*COI*<sup>V421A</sup>) resulting in a partial complex IV defect (Acin-Perez et al., 2003; Fan et al., 2008).

Here, we report the physiological effects of six nDNA-mtDNA combinations of wild-type (WT) and mutant nDNA *Ant1* and mtDNA *COI*<sup>V421A</sup> and *ND6*<sup>P25L</sup> alleles in C57BL/6J mice (Navarro et al., 2012). This investigation has established that mild differences in the mtDNA genotype can strongly influence the expressivity of autosomal gene mutations. Furthermore, the accumulation of somatic mtDNA mutations can

augment the consequences of unfavorable mitochondrial-nuclear interactions.

## RESULTS

### Transcriptional Profile of the *Ant1*-Deficient Heart

To clarify the molecular basis of the *Slc25a4* mutation-associated cardiomyopathy, we performed RNA sequencing on left ventricular myocardium of WT and *Ant1*<sup>-/-</sup> mice. Changes in functionally annotated gene families were assessed by gene set enrichment analysis. Significantly downregulated pathways included extracellular matrix, intracellular signaling, chemotaxis, and mitochondrial antioxidant and fatty acid metabolism genes (Figures 1A and S1). Upregulated pathways included mitochondrial OXPHOS enzymes, canonical skeletal muscle proteins, and membrane-associated voltage-gated ion channels (Figures 1B and S1).

The loss of structural extracellular components and the ectopic induction of skeletal muscle proteins in the myocardium are consistent with other forms of cardiomyopathy, as well as aging (Aronow et al., 2001; Houtkooper et al., 2011). The fibrotic alterations and cardiac remodeling from hypertrophic to dilated

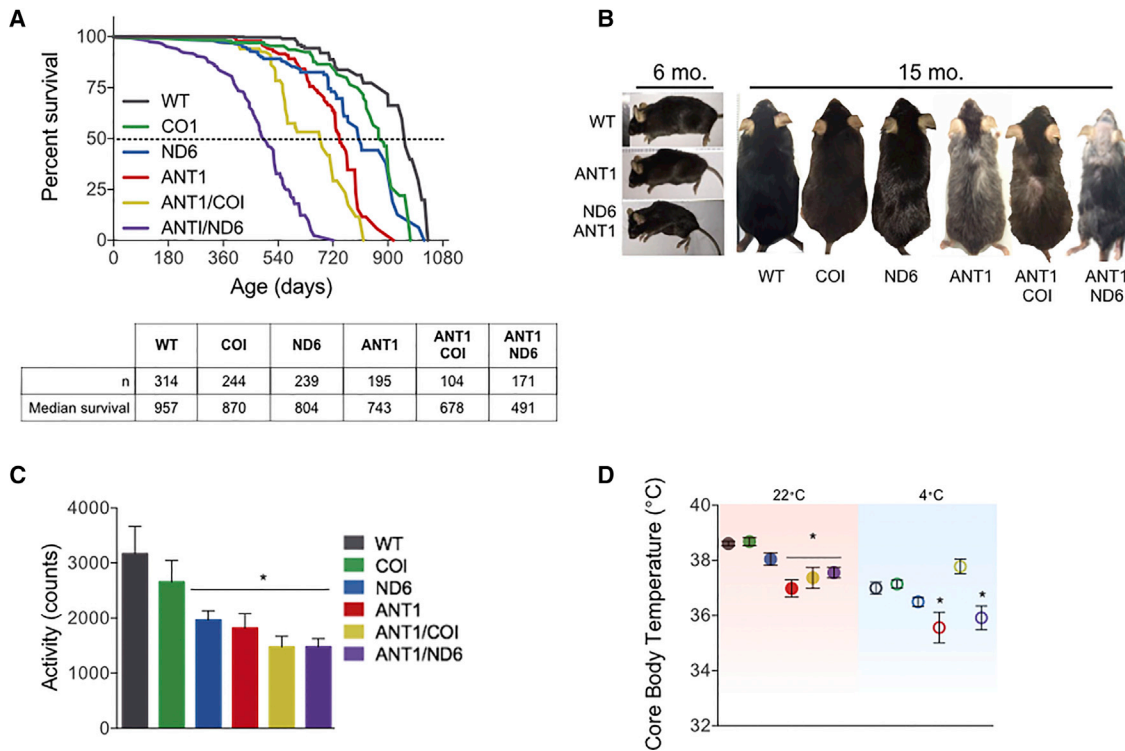


**Figure 2. Effects of Six nDNA-mtDNA *Ant1* and *COI*<sup>V421A</sup> and *ND6*<sup>P25L</sup> Combination Strains on Longevity, Activity, and Thermal Tolerance**

(A) Kaplan-Meier analysis of six nDNA-mtDNA combinations. Median lifespan and n are depicted in the chart below. (B) Progeroid morphology evident in *Ant1* and *ANT1/ND6* mice as early kyphosis at 6 months, which progresses to gray hair, alopecia, and advanced kyphosis at 15 months compared with WT and *ANT1/COI*. (C) Indirect calorimetry recordings of activity counts during the dark cycle of all strains at 6 months. (D) Core body temperature for 6-month-old mice measured at 22°C (filled symbols; red box) showing reduction of all *Ant1*-null strains. Core body temperature after 4°C cold stress (open symbols; blue box) showing that the *ANT1* and *ANT1/ND6* strains were unable to maintain normal body temperature while the *ANT1/COI* mice were unaffected by cold stress.

\*p < 0.02 versus WT; n = 6. See also Figure S2.

cardiomyopathy are also consistent with the observed pathology of the *Ant1*<sup>-/-</sup> mouse (Burke et al., 2016; Graham et al., 1997; Narula et al., 2011).

The induction of OXPHOS components is particularly noteworthy, with complex I (NADH-ubiquinone/plastoquinone oxidoreductase) genes being among the most strongly upregulated gene families in the *Ant1*-null heart (Figure 1B and Table S1). While the average change of all nDNA-coded OXPHOS polypeptide genes was slightly downregulated (Figure 1C), the mtDNA-coded OXPHOS complex I subunits were induced (Figures 1D and 1E). The preferential upregulation of mtDNA complex I genes may represent a compensatory response to a partial impairment of complex I by the *Ant1* mutation.

#### mtDNA Variants Alter *Ant1*<sup>-/-</sup> Murine Lifespan and the Response to Environmental Stress

Given the alterations in complex I expression induced by the *Ant1* mutation, we investigated the effects of combining the *Ant1* mutation with mtDNA mutations that resulted in partial defects in complex I, *ND6*<sup>P25L</sup>, versus complex IV, *COI*<sup>V421A</sup>. *Ant1* WT (*Ant1*<sup>+/+</sup>) and *Ant1* null (*Ant1*<sup>-/-</sup>) mice were crossed with mice harboring normal, *ND6*<sup>P25L</sup>, or *COI*<sup>V421A</sup> mtDNAs. This resulted in six nDNA-mtDNA combinations: WT nDNA and

WT mtDNA (WT); WT nDNA and *ND6*<sup>P25L</sup> mtDNA (ND6); WT nDNA and *COI*<sup>V421A</sup> mtDNA (COI); *Ant1*<sup>-/-</sup> and WT mtDNA (ANT1); *Ant1*<sup>-/-</sup> and *ND6*<sup>P25L</sup> mtDNA (ANT1/ND6); and *Ant1*<sup>-/-</sup> and *COI*<sup>V421A</sup> mtDNA (ANT1/COI). In all cases, the nDNA background was derived from C57BL/6J into which the WT *Nnt* allele was reintroduced (C57BL6/JEiJ) (Navarro et al., 2012).

In isolation, the *Ant1*<sup>-/-</sup>, *ND6*<sup>P25L</sup>, and *COI*<sup>V421A</sup> mutations had a modest effect on mouse longevity relative to WT: the *COI*<sup>V421A</sup> variant reduced lifespan by 9%, the *ND6*<sup>P25L</sup> variant by 16%, and the *Ant1*<sup>-/-</sup> by 22%. Combining the *Ant1*<sup>-/-</sup> with the *COI*<sup>V421A</sup> variant had minimal effect on the *Ant1*<sup>-/-</sup> lifespan, but combining the *Ant1*<sup>-/-</sup> with *ND6*<sup>P25L</sup> reduced the lifespan by 49%, more than twice that of the *Ant1*<sup>-/-</sup> alone (Figure 2A). Therefore, combining *Ant1*<sup>-/-</sup> with the *ND6*<sup>P25L</sup> variant was significantly more deleterious than combining *Ant1*<sup>-/-</sup> with *COI*<sup>V421A</sup>.

The *ANT1* and *ANT1/ND6* mice exhibited morphological features of premature aging starting with kyphosis at 6 months (Figure 2B), but *COI*, *ND6*, and *ANT1/COI* were indistinguishable from WT (not shown). By 15 months, *ANT1* and *ANT1/ND6* mice had pronounced kyphosis, gray hair, and alopecia, while *ANT1/COI* mice appeared less affected (Figure 2B). Basal motor activity levels of the *ND6*, *ANT1*, *ANT1/COI*, and *ANT1/ND6* mice were

significantly reduced in young mice, but COI mice were again indistinguishable from WT (Figure 2C).

To assess the effects of nDNA-mtDNA interaction on thermoregulation, core body temperature was first determined in mice housed at 22°C, which is ~10°C lower than their thermoneutral zone. This mild stress demands an ~60% increase in metabolic rate to maintain thermoregulation relative to thermoneutral temperature (Cannon and Nedergaard, 2011). WT, COI, and ND6 mice maintained their core body temperature under these standard housing conditions. However, the core body temperatures of ANT1, ANTI/COI, and ANTI/ND6 mice were reduced by an average of ~1.3°C relative to WT (Figure 2D). Of note, the body weights of these mice were indistinguishable (Figure S2). Metabolic stress was then increased by lowering the temperature to 4°C for 6 hr. Core body temperature of WT, COI, and ND6 mice decreased 1°C–2°C, while the ANT1 and ANTI/ND6 mice lost ~3°C (Figure 2D). Surprisingly, the ANTI/COI strain maintained the same core body temperature in these extreme conditions as at 22°C ( $\Delta 0.31^\circ\text{C} \pm 0.07^\circ\text{C}$ ). Hence, the *Ant1* mutation has the greatest impact on thermoregulation in mild conditions, which is sustained by the mtDNA *ND6*<sup>P25L</sup>, but ameliorated by the mtDNA *COI*<sup>V421A</sup> variant under more extreme environmental stress.

### mtDNA Variation Alters the Expressivity of Age-Dependent Cardiomyopathy

Since ANT1-deficient humans (Strauss et al., 2013) and mice (Narula et al., 2011) manifest age-related, progressive cardiomyopathy, we next investigated the relative cardiac weight and morphology of the six nDNA-mtDNA mouse strains over their lifespans (Figure 3A). The relative heart weight of WT mice increased  $0.06 \pm 0.008 \text{ mg g}^{-1} \cdot \text{month}^{-1}$  ( $r^2 = 0.32$ ;  $p < 0.0001$ ). The mtDNA *COI*<sup>V421A</sup> variant did not perturb this trend ( $p = 0.32$ ), while the *ND6*<sup>P25L</sup> variant reduced the WT rate by ~21% ( $p = 0.0003$ ; Figure 3A).

Deletion of *Ant1* increased the rate and extent of the age-related cardiac hypertrophy (Figure 3A). Again, the *COI*<sup>V421A</sup> variant did not affect this trend ( $p = 0.18$  for ANTI/COI versus ANT1). However, combination of *ND6*<sup>P25L</sup> with *Ant1*<sup>-/-</sup> accelerated the rate of cardiac enlargement ~200% over that of the *Ant1*<sup>-/-</sup> hearts ( $p = 0.003$ ). By 15 months, the relative heart weight of the ANTI/ND6 mice had increased 6.5-fold due to hypertrophic dilation (Figure 3B).

To further delineate the structural and functional consequences in the heart of each nDNA-mtDNA combination, we employed echocardiography (ECG) with M mode and speckle tracking in B mode for strain analysis. Strain reflects the total deformation of the ventricular myocardium during a cardiac cycle as a percentage of its initial length. Speckle-tracking-based strain analysis detects intrinsic contractile function, allowing assessment of myocardial pathophysiology prior to overt cardiac dysfunction (Biering-Sorensen et al., 2017; Geyer et al., 2010). Notably, there were no significant differences in mice harboring either the mtDNA *COI*<sup>V421A</sup> or *ND6*<sup>P25L</sup> variant related to WT across all ECG parameters examined (Table S2). The mtDNA variants only affected cardiac structure or function when the nDNA *Ant1* defect was also present. Addition of *COI*<sup>V421A</sup> to *Ant1*<sup>-/-</sup> decreased left ventricular posterior wall thickness at systole (PWTs), but had no functional conse-

quences on the *Ant1*<sup>-/-</sup> heart. Conversely, addition of the *ND6*<sup>P25L</sup> (ANTI/ND6) adversely affected every ECG measure, leading to dramatic ventricular dilation and an 80% reduction in cardiac contractility (Figure 3C; Table S2). Thus, the mtDNA *ND6*<sup>P25L</sup> variant markedly increased the severity of the *Ant1*<sup>-/-</sup> cardiomyopathy, while the mtDNA *COI*<sup>V421A</sup> variant had no effect.

### Opposing Effects of mtDNA *ND6*<sup>P25L</sup> and *COI*<sup>V421A</sup> on Mitochondrial Morphology

Abnormal mitochondrial morphology is commonly found in primary mitochondrial diseases, as well as in idiopathic cardiomyopathies. To determine how these genetic alterations could influence mitochondrial morphology within the heart, we performed ultrastructural analysis of the left ventricle. The results revealed highly disordered myofibrils in all but the WT and COI strains (Figures 4A–4F), altered mitochondrial morphology (Figures 4A'–4F'), and increased lipofuscin aggregates (Figure 4G) in strains with the shortest lifespan. While the mtDNA variants alone did not significantly alter mitochondrial content, *Ant1*<sup>-/-</sup> led to a 60% increase in mitochondrial number (Figure 4H), and ANTI/COI and ANTI/ND6 hearts had over twice the amount of mitochondria as WT (Figure 4H). ND6, ANT1, and ANTI/ND6 ventricles had increased mitochondrial fragmentation, with the ANTI/ND6 mitochondria reduced to half the size of all other strains (Figures 4I, 4J, and S3). Notably, the *COI*<sup>V421A</sup> variant had the reverse effect, leading to significant mitochondrial enlargement, which counterbalanced mitochondrial fragmentation in the *Ant1*<sup>-/-</sup> heart ( $p = 0.64$  for ANTI/COI versus WT; Figures 4I and S3).

While the WT, COI, and ND6 strains had similar intramitochondrial ultrastructure, all of the *Ant1*<sup>-/-</sup> strains were highly abnormal. The most common intramitochondrial abnormalities were electron dense inclusions, hypodense compartments, and cristae malformations (Figures 4K–4O and S4). Cristae morphology regulates mitochondrial functions that are crucial for cardiac homeostasis, such as respiratory efficiency, Ca<sup>2+</sup> buffering, reactive oxygen species (ROS) release, and apoptotic signaling (Cogliati et al., 2016). Accordingly, the strains with the most severe dilated cardiomyopathy (ANT, ANT/COI, and ANT/ND6) had the highest percentage of mitochondria with irregular cristae morphology (Figures 4L–4O and S4). The incidence of abnormal cristae was consistently higher in the ANTI/ND6 mitochondria than the ANTI/COI mitochondria.

### Functional OXPHOS Consequences of *Ant1* and mtDNA Mutations

Modulation of cristae morphology allows mitochondrial OXPHOS machinery to adapt to cellular substrate supply and metabolic demand by shifting form to meet function. The master regulator of cristae dynamics is the dynamin-related GTPase OPA1 (Glytsou et al., 2016). OPA1 localizes to the IMM, where its multiple isoforms coordinate mitochondrial fusion, cristae integrity, respiratory complex assembly and function, and mtDNA maintenance (Chen et al., 2012; Cogliati et al., 2013). When OPA1 is lost, or the isoforms are imbalanced, mitochondria fragment, undergo cristolysis, and OXPHOS assembly fails. Moreover, OPA1 overexpression proves protective for mitochondrial disease by correcting cristae structure and restoring

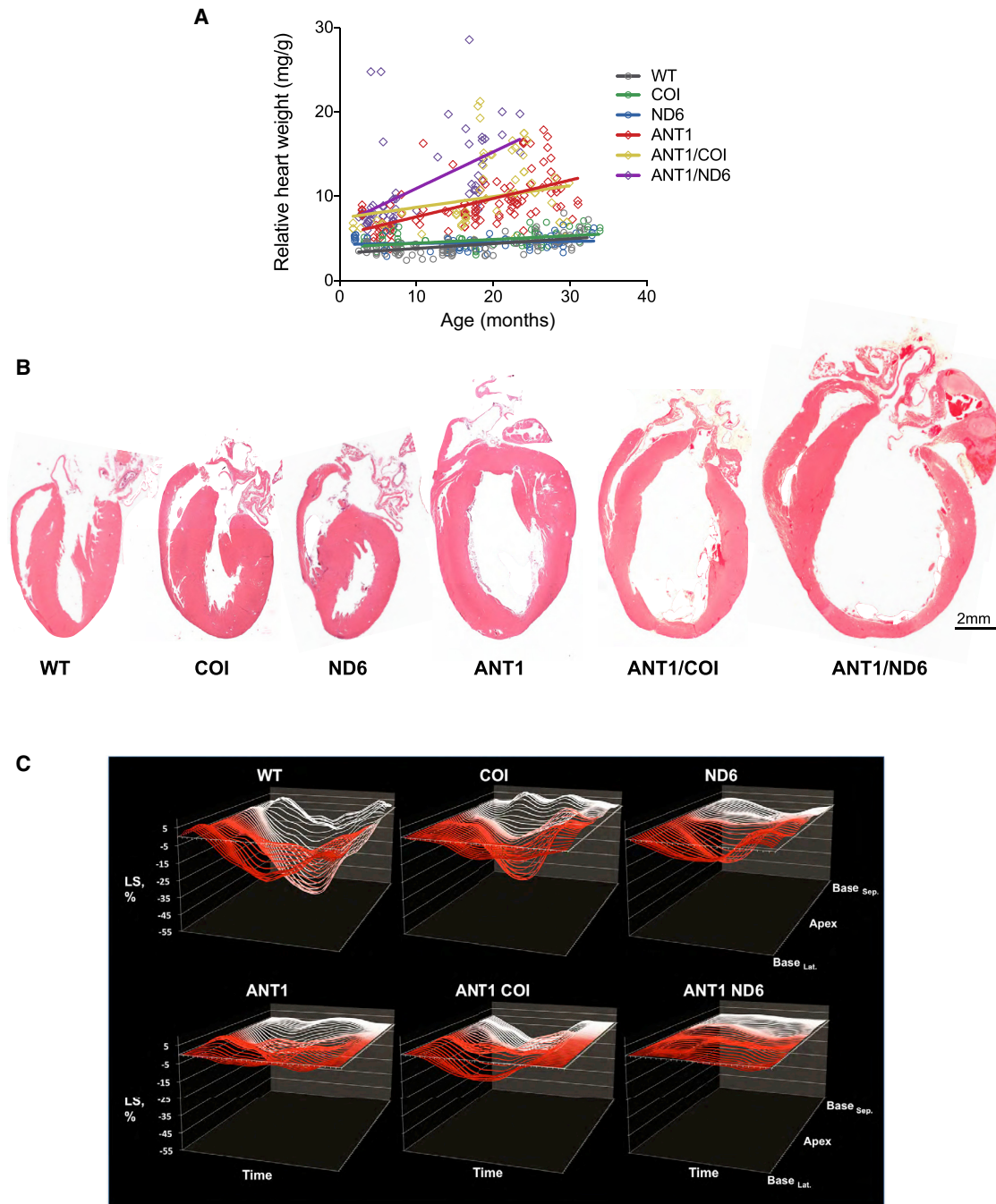


**Figure 3. Progression of Cardiomyopathy and Left Ventricular Mechanics in the nDNA-mtDNA Combination Strains**

(A) Correlation between the relative rate of cardiac enlargement (heart weight/body weight) over the lifespan for each strain ( $p < 0.0001$ ;  $n = 65-111$ ).

(B) Gross morphology of hearts by H&E stain at 12 months of age.

(C) Cardiac contractility measured by two-dimensional speckle-tracking echocardiography (2D-STE). Representative strain curves obtained from the B-mode long-axis view of the left ventricle over the cardiac cycle (x axis) showing longitudinal strain (% deformation; y axis) and region of the left ventricle (z axis). Each panel shows 49 regional strain curves topographically extending from infero-lateral base (Base<sub>Lat.</sub>) toward LV apex and back toward antero-septal base (Base<sub>Sep.</sub>). Note the progressive variations in magnitude and timing of the strain curves between different nDNA-mtDNA combinations.  $n = 10-34$ .

See also [Table S2](#).

OXPHOS function (Civiletto et al., 2015). To determine if altered OPA1 was associated with ultrastructural variation between the different nDNA-mtDNA combinations, OPA1 levels were quanti-

fied in cardiac mitochondria from each strain (Figure 5A). The presence of *ND6*<sup>P25L</sup> or *Ant1*<sup>-/-</sup> was associated with decreased OPA1 (Figure 5B), attributable to the specific loss of long OPA1

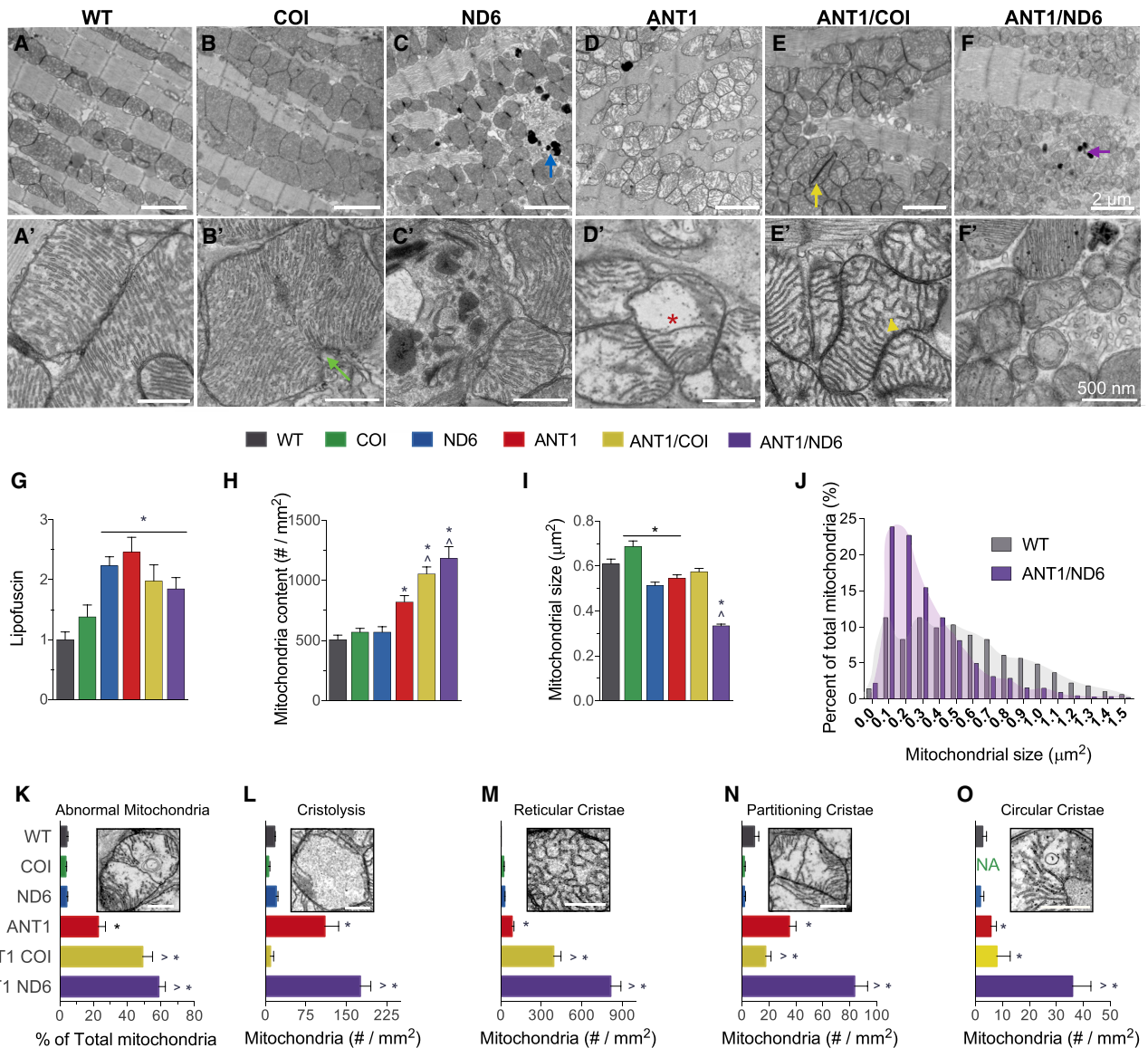


**Figure 4. Oposing Effects of mtDNA Variation in Complexes I and IV on Mitochondrial Morphology and Cristae Architecture**

(A–F) Representative electron micrographs of (A–F) ventricular cardiomyocytes and (A'–F') mitochondria from each nDNA-mtDNA combination (n = 3). Scale bars, 2  $\mu$ m (A–F); 500 nm (A'–F'). Sarcomeric and mitochondrial alignment in (A) WT and (B) COI versus structural disarray in all other nDNA-mtDNA combinations (C–F). (B and B') Mitochondrial enlargement in COI myocardium, suggestive of hyperfusion or impaired fission (green arrow; B'). Mitochondrial fragmentation, autophagic vesicles, and lipofuscin accumulation (blue and purple arrows) in (C and C') ND6 and (F and F') ANTI/ND6 myocardium. (D–F) Mitochondrial proliferation and (D'–F') cristae abnormalities, paracrystalline inclusions (yellow arrow; E, ANTI/COI), cristolysis (red asterisk; D', ANTI), and reticular morphology (yellow arrowhead; E', ANTI/COI), present in all *Ant1*-null strains.

(G–I) (G) Quantification of age-related lipofuscin deposits, normalized to WT. Ultrastructural quantification of (H) mitochondrial content and (I) average size per strain (n = 496–1,541).

(J) Percentage distribution of mitochondrial size showing the shift in mitochondrial morphology by the ANTI/ND6 compared with WT.

(K) Percent of abnormal mitochondria counted in each strain.

(L–O) Average number of mitochondria per  $\text{mm}^2$  with the following most common defects in cristae: (L) cristolysis, and (M) reticular, (N) partitioning, and (O) circular morphologies.

\*p < 0.05 versus WT; ^p < 0.001 versus ANTI. Data are represented as means  $\pm$  SE. See also Figures S3 and S4.

isoforms (I-OPAs; Figure 5C). Conversely, *COI*<sup>V421A</sup> mitochondria maintained OPA1 levels equivalent to WT, and blocked the loss of I-OPA1 associated with *Ant1*<sup>-/-</sup>.

Loss of OPA1 and cristae integrity are associated with an age-dependent decrease in the specific activities and assembly of

OXPHOS complexes I, IV, and V (Chen et al., 2012; Cogliati et al., 2013; Patten et al., 2014). To evaluate this relationship in the six nDNA-mtDNA combination strains, we analyzed the activity, amount, and structural assembly of these heart OXPHOS complexes. The *ND6*<sup>P25L</sup> variant decreased complex I (C-I),

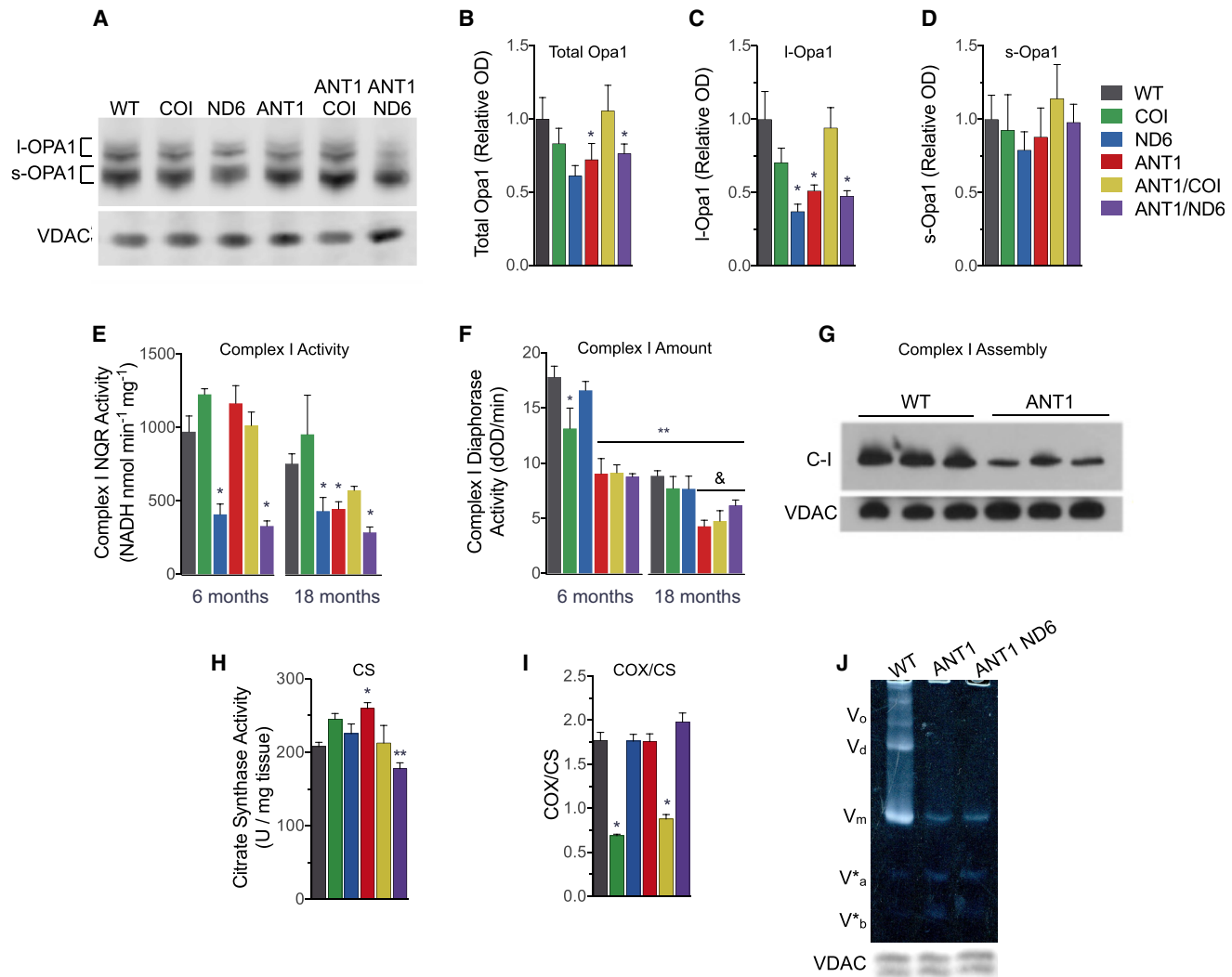


**Figure 5. Consequences of Mitochondrial-Nuclear Interaction on OPA1 Processing and Mitochondrial OXPHOS Complexes**  
 (A–D) (A) Representative western blot of OPA1 and VDAC from isolated heart mitochondria. Densitometric analysis of (B) total OPA1, (C) long Opa1 (I-OPA1), and (D) short OPA1 (s-OPA1) isoforms, normalized to VDAC and shown as fold change from WT.  
 (E and F) (E) Complex I (C-I) NADH:quinone oxidoreductase (NQR) activity determined by rotenone-sensitive NADH oxidation in the presence of coenzyme Q<sub>1</sub> using isolated heart mitochondria (25 μg). (F) Age-dependent decline in C-I diaphorase activity (dOD/min) determined by C-I immunocaptured from 10 μg of isolated heart mitochondria (\*\*p < 0.0001 versus WT at 6 months; \*p < 0.05 versus WT at 18 months).  
 (G) C-I assembly measured by blue native electrophoresis of heart mitochondria (20 μg) and immunodetection with anti-NDUFA1.  
 (H) Citrate synthase (CS) activity per mg myocardial tissue as a marker of mitochondrial content at 6 months (\*\*p < 0.01 versus ANT1).  
 (I) Cytochrome c oxidase (COX) activity from the same samples normalized to CS activity. Data are represented as means ± SE.  
 (J) Resolution of oligomeric states of complex V (C-V) F<sub>1</sub>F<sub>0</sub>-ATPase by clear native PAGE. Oligomers were undetectable in *Ant1*<sup>-/-</sup> mitochondria solubilized in digitonin (3% w/v). V<sub>0</sub>, oligomers; V<sub>d</sub>, dimers; V<sub>m</sub>, monomers; V<sup>\*</sup><sub>a</sub> and V<sup>\*</sup><sub>b</sub>, partial C-V components. Each well was loaded with 30 μg of mitochondrial protein, evident by the anti-VDAC loading control from a duplicate gel.  
 \*p ≤ 0.05, \*\*p < 0.001 versus age-matched WT, except as noted in (F) and (H); n = 3–7. See also Figure S5.

rotenone-sensitive, NADH:quinone oxidoreductase (NQR) specific activity by 58% in 6-month-old mice (Figure 5E), which was reduced an additional 10% when combined with *Ant1*<sup>-/-</sup>. At 18 months of age, C-I NQR activity in the ANT1 heart was decreased to the same low level as the ND6, and their combination (ANT1/ND6) decreased C-I NQR activity an additional ~50% (Figure 5E). In contrast, C-I NQR activity in the COI mice remained normal at both 6 and 18 months, and C-I activity in the ANT1/COI heart was higher than that of the ND6, ANT1, or

ANT1/ND6 hearts at 18 months (Figure 5E). *COI*<sup>V421A</sup> also increased C-I subunits in *Ant1*<sup>-/-</sup> hearts at 6 months of age and prevented the age-associated loss of C-I subunits that occurred in all other nDNA-mtDNA mutant strains (Figure S5). Thus, the *COI*<sup>V421A</sup> mtDNA variant partially compensates for the *Ant1*<sup>-/-</sup> complex I defect.

To determine whether the decline in NQR activity could be attributed to a decreased amount of C-I, we measured the diaphorase activity of holoenzyme C-I (Figure 5F). While *ND6*<sup>P25L</sup>

decreased C-I NQR specific activity by half, this variant had no effect on the amount of holoenzyme (Figure 5F). Surprisingly, *Ant1*<sup>-/-</sup> reduced holoenzyme levels by ~51% in 6-month-old hearts without affecting NQR specific activity. Both age and genotype significantly influenced C-I content, accounting for 42% and 34% of the total variance, respectively, but age was the dominant factor ( $p < 0.0001$ ; two-way ANOVA for age  $\times$  genotype). The decreased amount of assembled C-I in ANT1 hearts was confirmed by blue native gel electrophoresis (Figure 5G).

Complex IV (COX) activity was measured by cytochrome c oxidation in myocardial homogenates, and the specific activity normalized to citrate synthase (CS) activity (Figures 5H and 5I). CS activity was increased by 25% in *Ant1*-deficient myocardium but decreased by the addition of *ND6*<sup>P25L</sup> (Figure 5H). COX/CS activity was decreased to 39% of control by the mtDNA *COI*<sup>V421A</sup> mutation, but the additional loss of *Ant1* (ANT1/COI) had no appreciable effect. *Ant1*<sup>-/-</sup>, *ND6*<sup>P25L</sup>, or their combination, had no effect on the COX/CS activity up to 18 months of age (Figure 5I).

Since all *Ant1*<sup>-/-</sup> hearts have an abnormal cristae structure, which is only partially alleviated by the retention of I-Opa1 in ANT1/COI mitochondria, and complex V ( $F_1F_0$ -ATPase) dimerization is obligatory for proper cristae formation (Davies et al., 2012; Paumard et al., 2002; Strauss et al., 2008), we hypothesized that  $F_1F_0$ -ATPase structural assembly might be affected by loss of *Ant1*. The dimer equilibrium of the  $F_1F_0$ -ATPase was determined by clear native gel electrophoresis under mild solubilizing conditions (Wittig et al., 2010).  $F_1F_0$ -ATPase dimers and oligomers were drastically decreased in ANT1 and ANTI/ND6 heart mitochondria (Figure 5J). Analysis using more stringent detergent revealed that the ATP synthase monomers (V) are also labile and give rise to subcomplexes V\*a and V\*b in all *Ant1*<sup>-/-</sup> hearts (Figure S5), which resemble those reported in cells harboring mtDNA *ATP6* and *ATP8* mutations (Carrozzo et al., 2006; Mourier et al., 2014; van der Westhuizen et al., 2010).

### Mitochondrial Respiration, ROS Production, and mtPTP Activation

To determine how these genetic defects alter mitochondrial physiology, we analyzed isolated heart mitochondria from 6- to 18-month-old animals. *Ant1*<sup>-/-</sup> increased the mitochondrial membrane potential ~25%–30% in young ANT1, ANT1/COI, and ANT1/ND6 hearts relative to WT, COI, and ND6 hearts (Figure 6A), possibly due to the subassembled  $F_1F_0$ -ATPase (Mourier et al., 2014) or its diminished activity due to limited availability of matrix ADP (Graham et al., 1997).

Oxygen consumption was then measured in heart mitochondria respiring on the C-I, NADH-linked substrates glutamate and malate (GM). The mtDNA mutations affected different aspects of mitochondrial respiration: *COI*<sup>V421A</sup> impaired the LEAK (L) state (in the absence of ADP or uncoupler; Figure 6B), while *ND6*<sup>P25L</sup> impaired the ADP-stimulated (P) state (Figure 6C). Interestingly, *Ant1*<sup>-/-</sup> did not impair ADP-stimulated respiration in young animals, possibly due to compensation by ANT2 (Brand et al., 2005).

To determine the importance of the  $F_1F_0$ -ATPase on state III (ADP-stimulated; P) respiration, we treated mitochondria respiring on GM and ADP with the  $F_1F_0$ -ATPase inhibitor oligomycin. Oligomycin decreased the state III respiration rate of

WT, COI, and ND6 mitochondria 80%, consistent with mitochondrial respiration being predominantly coupled to the  $F_1F_0$ -ATPase through use of the proton gradient to synthesize ATP (Figure 6D). Conversely, oligomycin only decreased *Ant1*-null mitochondrial respiration by 50%–60% (Figure 6D). The diminished effect of oligomycin may be due to the preexisting inhibition of respiration due to limited mitochondrial ADP import caused by the loss of ANT1 and impaired  $F_1F_0$ -ATPase function and assembly (Mourier et al., 2014).

To determine how the nDNA-mtDNA genetic combinations influence mitochondrial ROS production in the heart, we analyzed  $H_2O_2$  emission using the Amplex red assay (Figure 6E). When mitochondria were respiring on GM,  $H_2O_2$  emission was increased 18%–48% in mitochondria harboring the *COI*<sup>V421A</sup> variant, as well as all *Ant1*-null mitochondria (Figure 6E, GM). Treatment with rotenone (R), which binds to the C-I CoQ binding site downstream of the site of NADH reduction and enhances ROS production via forward electron transport (FET) (Murphy, 2009), decreased *COI*<sup>V421A</sup> ROS production but increased *ND6*<sup>P25L</sup> ROS production. When the complex II substrate, succinate, is added as the electron donor and the membrane potential maximized by blocking the  $F_1F_0$ -ATPase with oligomycin, the electrons are driven backward from CoQ into C-I, resulting in ROS production by reverse electron transport (RET) (Brand, 2010; Chouchani et al., 2014; Murphy, 2009). In this case, ROS production from ND6 and ANTI/ND6 heart mitochondria was abolished (Figure 6E, Succ + Oligo). By contrast, WT, ANT1, and COI mitochondria showed robust ROS production by RET. To determine if these different modes of ROS production were associated with oxidative stress *in vivo*, we measured 3-nitrotyrosine protein adducts and found the highest level of oxidative damage in ANT1/ND6 hearts, which only produce ROS by FET (Figure 6F).

Excessive mitochondrial ROS production via FET induces ryanodine receptor-dependent  $Ca^{2+}$  release and sensitizes the mtPTP, which impairs cardiac contractility and increases mitochondrial permeability transition (Zorov et al., 2000). Since ANTI/ND6 hearts have the most diminished contractility and the highest FET-associated ROS and oxidized proteins, we hypothesized that their mitochondria would also be most susceptible to  $Ca^{2+}$ -mediated permeability transition. Indeed, the addition of *ND6*<sup>P25L</sup> to *Ant1*<sup>-/-</sup> increased  $Ca^{2+}$  sensitivity of the mtPTP, rendering ANTI/ND6 hearts more prone to permeability transition (Figures 6G and 6H) and the release of apoptogenic proteins into the cytosol, culminating in effector caspase activation (Figure 6I) (McManus et al., 2014).

### mtDNA Somatic Mutation Load Correlates with the Progression of *Ant1*<sup>-/-</sup> Cardiomyopathy

Since the ANT1 and COI and ND6 alterations are present at birth, the progression of the cardiomyopathy of the ANTI/ND6 mutant heart implies the presence of an additional age-related mitochondrial factor. We hypothesized that this additional factor may be the accumulation of somatic mtDNA mutations due to persistent oxidative stress and/or impaired mitochondrial turnover (Dai et al., 2010). We analyzed the relative levels of deleted mtDNAs in ventricular tissue from the six nDNA-mtDNA combinations using long extension PCR (LX-PCR) (Figures 7A and 7B) and random mutation capture quantitative PCR (Figure 7C)

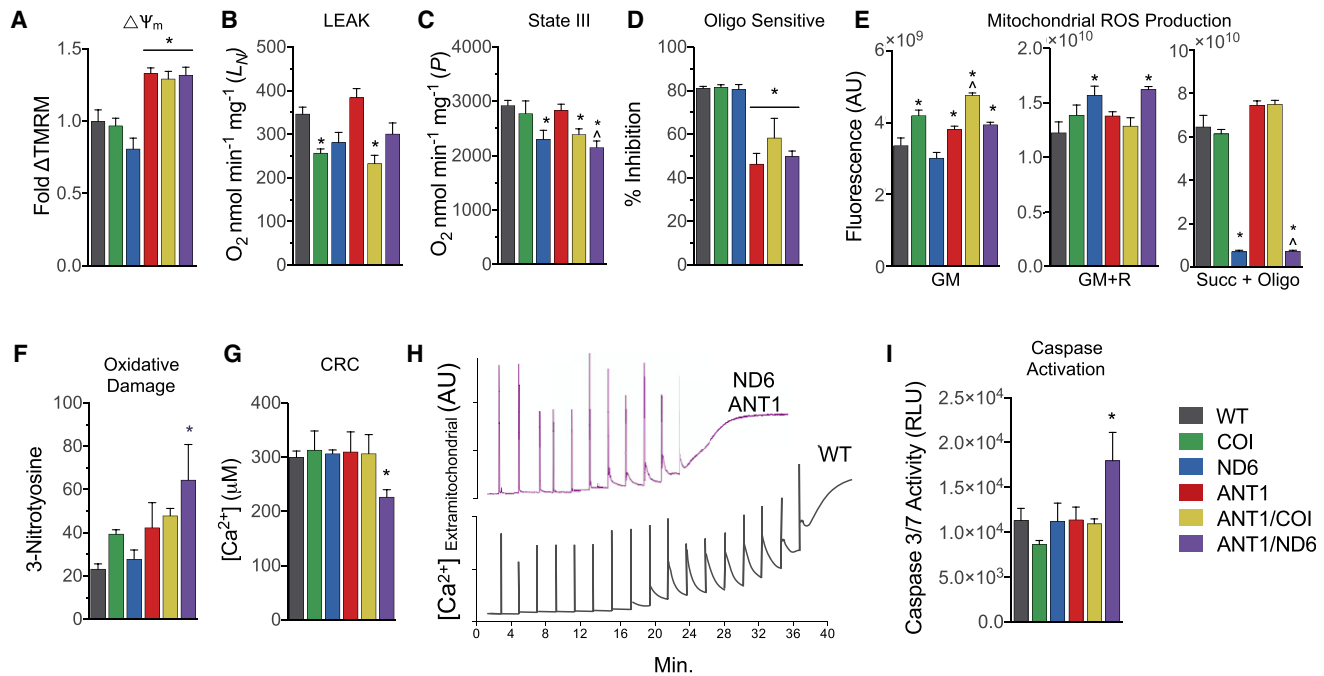


**Figure 6. Mitochondrial Bioenergetics, ROS Production, and mtPTP Stability in Isolated Cardiac Mitochondria from Six nDNA-mtDNA Genetic Combinations**

(A) Mitochondrial membrane potential determined by tetramethylrhodamine methyl ester fluorescence respiring on glutamate and malate (GM), graphed relative to WT.  
 (B) Mitochondrial oxygen consumption rate metabolizing glutamate and malate (GM) in the absence of ADP or uncoupler (state II or LEAK rate).  
 (C) Mitochondrial oxygen consumption rate metabolizing GM in the presence of ADP (state III or *P* rate).  
 (D) Relative inhibition of respiration by oligomycin in mitochondria during state III.  
 (E) Hydrogen peroxide ( $H_2O_2$ ) production detected by Amplex red in isolated mitochondria incubated with GM, rotenone (R), or succinate (Succ) and oligomycin (Oligo).  
 (F) Nitroxidative damage determined by 3-nitrotyrosine (3NT) protein adducts in heart tissue from 12-month-old mice.  
 (G)  $Ca^{2+}$  levels required to activate the mtPTP and collapse the mitochondrial membrane potential.  
 (H) Representative traces of extramitochondrial  $Ca^{2+}$  following 20  $\mu M$   $Ca^{2+}$  pulses delivered every 2 min until the spontaneous release of mitochondrial  $Ca^{2+}$ , marking the onset of mtPTP opening in WT and ANTI/ND6 mice.  
 (I) Activation of intrinsic apoptosis determined by effector caspase-3 and -7 activities.

Data are represented as means  $\pm$  SE. \* $p \leq 0.01$  versus WT; ^ $p \leq 0.01$  versus ANTI1;  $n = 3-5$ . See also Figure S6.

(Vermulst et al., 2007, 2008a, 2008b). The frequency of mtDNA deletions per mitochondrial genome increased linearly over time in all strains (Figure 7C). The somatic mtDNA mutation rate was 2-fold higher in ANTI hearts and almost 6-fold higher in ANTI/ND6 hearts (versus WT,  $p < 0.01$ ), which correlated with increased COX-deficient myocardial fibers (Figure S7), and severity of cardiomyopathy and mortality induced by the different mtDNA-nDNA combinations (Figures 7D and 7E).

## DISCUSSION

The goal of this study was to determine whether mtDNA is a crucial modulator of autosomal gene mutations with variable expressivity and to provide insight into how mitochondrial-nuclear interactions contribute to cardiovascular disease and heart failure (Arbustini et al., 1998b; Strauss et al., 2013). We first confirmed that mtDNA variants can modulate the expressivity of nDNA gene mutations by analyzing cardiac function and mitochondrial physiology of mice sharing the nuclear *Ant1* null mutation (Graham et al., 1997; Narula et al., 2011), but with different mtDNAs (WT,  $ND6^{P25L}$ , or  $COI^{V421A}$ ). Importantly, neither the

mtDNA  $ND6^{P25L}$  nor  $COI^{V421A}$  variant alone has an appreciable effect on cardiac physiology in C57BL/6J mice. The  $COI^{V421A}$  variant also has minimal effect on the *Ant1*<sup>-/-</sup> cardiac pathophysiology. By contrast, the mtDNA  $ND6^{P25L}$  variant accelerates the *Ant1*<sup>-/-</sup> phenotype, resulting in a rapidly progressive, and ultimately fatal, dilated cardiomyopathy. The markedly different effects of the  $COI^{V421A}$  and  $ND6^{P25L}$  variants on *Ant1*<sup>-/-</sup>-induced cardiomyopathy is proof of principle that mtDNA can exert modifier effects on the expressivity of autosomal gene mutations.

Further evidence that nDNA-mtDNA interactions can affect the severity of cardiomyopathy is found in our concurrent discovery that the nDNA *Nnt* genotype exerts a marked modifier effect on the cardiac phenotype of the mtDNA  $COI^{V421A}$  variant. C57BL/6J mice are homozygous for a truncated *Nnt* allele (*Nnt*<sup>-/-</sup>), which itself causes no overt cardiac defects in mice (Freeman et al., 2006; Huang et al., 2006; Toye et al., 2005). As we reported previously, the mtDNA  $COI^{V421A}$  variant on the C57BL/6J *Nnt*<sup>-/-</sup> background causes hypertrophic cardiomyopathy (Fan et al., 2008). However, when the mtDNA  $COI^{V421A}$  was transferred onto the C57BL/6J *Nnt*<sup>+/+</sup> nuclear background, the  $COI^{V421A}$  variant had little effect on the cardiac function (Figure 3C).

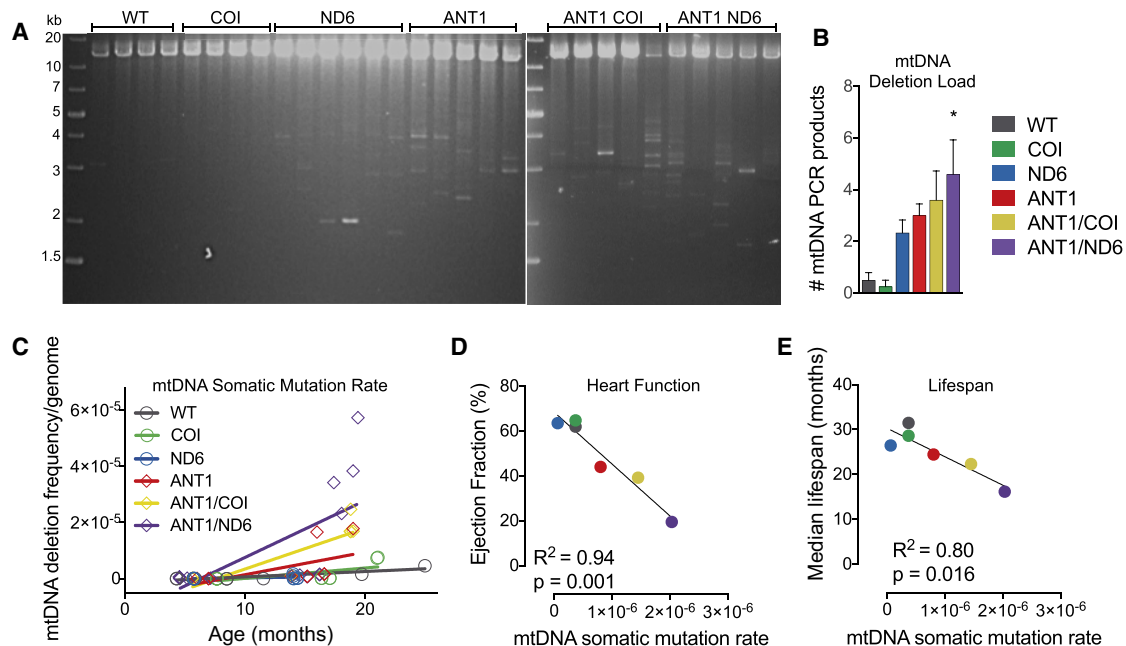


**Figure 7. Effect of Mitochondrial-Nuclear Interaction on Somatic mtDNA Mutation Accumulation**

(A and B) Long-range amplification of mtDNA (12.7 kb) from each nDNA-mtDNA combination at 12–15 months indicating multiple, large-scale deletions (\*p = 0.01; n = 4–6).

(C) Linear regression analysis of the frequency of mtDNA deletions per genome detected by qPCR of the most common deletion hotspot flanking two 15-bp repeats in mtDNA of mice from each strain over 4–25 months of age (p < 0.001; n = 8–14).

(D and E) Correlation between (D) median lifespan or (E) cardiac function and the mtDNA somatic mutation rate, as determined by random mutation capture assay.

See also Figure S7.

Hence, the *COI*<sup>V421A</sup> variant acts synergistically with the *Nnt*<sup>-/-</sup> null mutation, while the *ND6*<sup>P25L</sup> mutation acts synergistically with the *Ant1*<sup>-/-</sup> null mutation.

Having established that mitochondrial-nuclear interactions do modulate both mtDNA and nDNA expressivity, we investigated the pathophysiological basis of this relationship. Our analysis revealed four major mechanisms by which mtDNA variation modulates *Ant1* expressivity: OXPHOS complex I function, differential ROS production, mPTP sensitivity, and the somatic mtDNA mutation rate. First, *Ant1*<sup>-/-</sup> and *ND6*<sup>P25L</sup> both perturb complex I, with *Ant1*<sup>-/-</sup> reducing the amount of structurally assembled complex I, and the *ND6*<sup>P25L</sup> variant reducing complex I specific activity. Second, the *ND6*<sup>P25L</sup> variant generates comparable total ROS production as *Ant1*<sup>-/-</sup> and *COI*<sup>V421A</sup>, but the *ND6*<sup>P25L</sup> variant produces ROS only by FET, as opposed to both FET and RET for the *Ant1*<sup>-/-</sup> and *COI*<sup>V421A</sup> variants. ROS produced by RET induces mitochondrial hormesis, which is protective of age-related disease and extends lifespan (Scialo et al., 2016). Since *ND6*<sup>P25L</sup> blocks RET, this cytoprotective effect would be lost for the mtDNA *ND6*<sup>P25L</sup> but not for the *COI*<sup>V421A</sup>. Third, the *Ant1*<sup>-/-</sup>/*ND6*<sup>P25L</sup> combination sensitizes cardiac mitochondria to Ca<sup>2+</sup>-induced mtPTP permeability transition while the *Ant1*<sup>-/-</sup>/*COI*<sup>V421A</sup> combination does not, which is consistent with increased oxidative damage and defective cardiac contractility in the compound *Ant1*<sup>-/-</sup>/*ND6*<sup>P25L</sup> genotype (Zorov et al., 2000). Finally, the *Ant1*<sup>-/-</sup>/*ND6*<sup>P25L</sup> combination results in a 2.5-fold higher mtDNA somatic mutation rate than the *Ant1*<sup>-/-</sup>

*COI*<sup>V421A</sup> combination, which may amplify the inherited mitochondrial defects over time and accelerate the progression of cardiomyopathy (Vermulst et al., 2007, 2008b).

The distinctive alterations in mitochondrial ultrastructure conferred by the mtDNA variants are consistent with their respective biochemical consequences on *Ant1* expressivity, which appear to converge at the mitochondrial dynamics regulator, OPA1. The effect of mtDNA *COI*<sup>V421A</sup> and *ND6*<sup>P25L</sup> on mitochondrial morphology is diametrically opposed: *COI*<sup>V421A</sup> increases mitochondrial size, while *ND6*<sup>P25L</sup> causes severe mitochondrial fragmentation. Interestingly, *ND6*<sup>P25L</sup> and *Ant1*<sup>-/-</sup> each lead to loss of the long OPA1 isoforms (l-OPA1) responsible for mitochondrial fusion (Figure 5C), supporting a key role for complex I inhibition and ROS production in aberrant OPA1 processing and downstream mitochondrial fragmentation (Gray et al., 2013; Norton et al., 2014; Ramonet et al., 2013). Mitochondrial fragmentation not only induces more ROS and mtDNA damage (Yu et al., 2008), it also impairs the mixing of multiple mtDNAs within the same mitochondrion, thereby blocking the benefits of inter-mtDNA complementation (Chen et al., 2010). Accordingly, increased *de novo* somatic mtDNA mutations due to *Ant1*<sup>-/-</sup> (Figures 7A–7C) would be more deleterious when combined with *ND6*<sup>P25L</sup> than with *COI*<sup>V421A</sup>. Indeed, the *COI*<sup>V421A</sup> variant prevents *Ant1*<sup>-/-</sup>-induced complex I impairment and loss of l-OPA1 and blocks mitochondrial fragmentation, thus preventing the decline in *Ant1*<sup>-/-</sup> mitochondrial function with age (Figure S6).

In conclusion, we have shown that the severity of the cardiomyopathy caused by a nuclear gene mutation can be directly modulated by the presence of otherwise sub-pathogenic mtDNA variants. This was true both for the differential effects of the *ND6<sup>P25L</sup>* and *COI<sup>V421A</sup>* mtDNA variants on the *Ant1<sup>-/-</sup>* background, as well as for the *COI<sup>V421A</sup>* versus WT mtDNA on the *Nnt<sup>-/-</sup>* background. These results demonstrate that nDNA-mtDNA interactions can play a critical role in modulating the phenotypes of nDNA gene mutations.

### Limitations of Study

While we feel that mtDNA-nDNA interactions will be important in modulating the manifestations of various nDNA gene mutations, the specific phenotypic manifestations described here undoubtedly reflect the specific mouse mtDNA sequences and the *Ant1<sup>-/-</sup>* mutant used in this study.

### STAR★METHODS

Detailed methods are provided in the online version of this paper and include the following:

- KEY RESOURCES TABLE
- CONTACT FOR REAGENT AND RESOURCE SHARING
- EXPERIMENTAL MODEL AND SUBJECT DETAILS
  - Mouse Genetics
  - Mouse Maintenance and Longevity
- METHOD DETAILS
  - RNA Sequencing and Bioinformatics
  - Cardiac Size and Histopathology
  - Calorimetry
  - Speckle Tracking Echocardiography of Left Ventricular Mechanics
  - Mitochondrial Morphology
  - Mitochondrial Isolation
  - Complex I Activity
  - Native Gel Electrophoresis and Immunodetection
  - Cytochrome-c Oxidase and Citrate Synthase Activity
  - Western Blotting and ELISA
  - Respiration
  - Mitochondrial Reactive Oxygen Species (mtROS) and Membrane Potential (MMP)
  - Calcium Retention Capacity
  - mtDNA Deletion Analysis
  - Caspase-3/7 Activity
  - COX-SDH Histochemistry
- DATA AND SOFTWARE AVAILABILITY
- QUANTIFICATION AND STATISTICAL ANALYSIS

### SUPPLEMENTAL INFORMATION

Supplemental Information includes seven figures and two tables and can be found with this article online at <https://doi.org/10.1016/j.cmet.2018.08.002>.

### ACKNOWLEDGMENTS

This work was supported by NIH grants 5R01-NS021328-30, 1R01MH108592-01A1, 1R01MN110185-01A1, R01NS41850, and R01OD010944-05 and DOD grant PR150585.

### AUTHOR CONTRIBUTIONS

M.J.M., H.-W.C., J.N., and D.C.W. designed the research; M.J.M., H.-W.C., M.P., H.J.H., P.P., A.T., A.A., R.M.M., and M.V. performed experiments; M.J.M., M.P., J.L., H.J.H., B.A.K., P.S., M.V., J.N., and D.C.W. analyzed the data; M.J.M., M.P., J.N., and D.C.W. wrote the paper.

### DECLARATION OF INTERESTS

The authors declare no competing interests.

Received: June 11, 2017

Revised: February 1, 2018

Accepted: August 1, 2018

Published: August 30, 2018

### REFERENCES

- Acin-Perez, R., Bayona-Bafaluy, M.P., Bueno, M., Machicado, C., Fernandez-Silva, P., Perez-Martos, A., Montoya, J., Lopez-Perez, M.J., Sancho, J., and Enriquez, J.A. (2003). An intragenic suppressor in the cytochrome c oxidase I gene of mouse mitochondrial DNA. *Hum. Mol. Genet.* *12*, 329–339.
- Arbustini, E., Diegoli, M., Fasani, R., Grasso, M., Morbini, P., Banchieri, N., Bellini, O., Dal Bello, B., Pilotto, A., Magrini, G., et al. (1998a). Mitochondrial DNA mutations and mitochondrial abnormalities in dilated cardiomyopathy. *Am. J. Pathol.* *153*, 1501–1510.
- Arbustini, E., Fasani, R., Morbini, P., Diegoli, M., Grasso, M., Dal Bello, B., Marangoni, E., Banfi, P., Banchieri, N., Bellini, O., et al. (1998b). Coexistence of mitochondrial DNA and beta myosin heavy chain mutations in hypertrophic cardiomyopathy with late congestive heart failure, [published erratum appears in *Heart* 1999 Mar;81(3):330]. *Heart* *80*, 548–558.
- Aronow, B.J., Toyokawa, T., Canning, A., Haghighi, K., Delling, U., Kranias, E., Molkentin, J.D., and Dorn, G.W., 2nd (2001). Divergent transcriptional responses to independent genetic causes of cardiac hypertrophy. *Physiol. Genomics* *6*, 19–28.
- Bauer, M.K., Schubert, A., Rocks, O., and Grimm, S. (1999). Adenine nucleotide translocase-1, a component of the permeability transition pore, can dominantly induce apoptosis. *J. Cell Biol.* *147*, 1493–1502.
- Biering-Sorensen, T., Biering-Sorensen, S.R., Olsen, F.J., Sengelov, M., Jorgensen, P.G., Mogelvang, R., Shah, A.M., and Jensen, J.S. (2017). Global longitudinal strain by echocardiography predicts long-term risk of cardiovascular morbidity and mortality in a low-risk general population: the Copenhagen City Heart Study. *Circ. Cardiovasc. Imaging* *10*, e005521.
- Brand, M.D. (2010). The sites and topology of mitochondrial superoxide production. *Exp. Gerontol.* *45*, 466–472.
- Brand, M.D., Pakay, J.L., Ocloo, A., Kokoszka, J., Wallace, D.C., Brookes, P.S., and Cornwall, E.J. (2005). The basal proton conductance of mitochondria depends on adenine nucleotide translocase content. *Biochem. J.* *392*, 353–362.
- Burke, M.A., Chang, S., Wakimoto, H., Gorham, J.M., Conner, D.A., Christodoulou, D.C., Parfenov, M.G., DePalma, S.R., Eminaga, S., Konno, T., et al. (2016). Molecular profiling of dilated cardiomyopathy that progresses to heart failure. *JCI Insight* *1*, e86898.
- Cannon, B., and Nedergaard, J. (2011). Nonshivering thermogenesis and its adequate measurement in metabolic studies. *J. Exp. Biol.* *214*, 242–253.
- Capaldi, R.A., Marusich, M.F., and Taanman, J.W. (1995). Mammalian cytochrome-c oxidase: characterization of enzyme and immunological detection of subunits in tissue extracts and whole cells. *Methods Enzymol.* *260*, 117–132.
- Carrozzo, R., Wittig, I., Santorelli, F.M., Bertini, E., Hofmann, S., Brandt, U., and Schagger, H. (2006). Subcomplexes of human ATP synthase mark mitochondrial biosynthesis disorders. *Ann. Neurol.* *59*, 265–275.
- Chen, H., Vermulst, M., Wang, Y.E., Chomyn, A., Prolla, T.A., McCaffery, J.M., and Chan, D.C. (2010). Mitochondrial fusion is required for mtDNA stability in skeletal muscle and tolerance of mtDNA mutations. *Cell* *141*, 280–289.

- Chen, L., Liu, T., Tran, A., Lu, X., Tomilov, A.A., Davies, V., Cortopassi, G., Chiamvimonvat, N., Bers, D.M., Votruba, M., et al. (2012). OPA1 mutation and late-onset cardiomyopathy: mitochondrial dysfunction and mtDNA instability. *J. Am. Heart Assoc.* *1*, e003012.
- Chevrollier, A., Loiseau, D., Reynier, P., and Stepien, G. (2011). Adenine nucleotide translocase 2 is a key mitochondrial protein in cancer metabolism. *Biochim. Biophys. Acta* *1807*, 562–567.
- Chouchani, E.T., Pell, V.R., Gaude, E., Aksentijevic, D., Sundier, S.Y., Robb, E.L., Logan, A., Nadtochiy, S.M., Ord, E.N., Smith, A.C., et al. (2014). Ischaemic accumulation of succinate controls reperfusion injury through mitochondrial ROS. *Nature* *515*, 431–435.
- Civiletto, G., Varanita, T., Cerutti, R., Gorletta, T., Barbaro, S., Marchet, S., Lamperti, C., Viscomi, C., Scorrano, L., and Zeviani, M. (2015). Opa1 overexpression ameliorates the phenotype of two mitochondrial disease mouse models. *Cell Metab.* *21*, 845–854.
- Cogliati, S., Enriquez, J.A., and Scorrano, L. (2016). Mitochondrial cristae: where beauty meets functionality. *Trends Biochem. Sci.* *41*, 261–273.
- Cogliati, S., Frezza, C., Soriano, M.E., Varanita, T., Quintana-Cabrera, R., Corrado, M., Cipolat, S., Costa, V., Casarin, A., Gomes, L.C., et al. (2013). Mitochondrial cristae shape determines respiratory chain supercomplexes assembly and respiratory efficiency. *Cell* *155*, 160–171.
- Dai, D.F., Chen, T., Wanagat, J., Lafamme, M., Marcinek, D.J., Emond, M.J., Ngo, C.P., Prolla, T.A., and Rabinovitch, P.S. (2010). Age-dependent cardiomyopathy in mitochondrial mutator mice is attenuated by overexpression of catalase targeted to mitochondria. *Aging Cell* *9*, 536–544.
- Davies, K.M., Anselmi, C., Wittig, I., Faraldo-Gomez, J.D., and Kuhlbrandt, W. (2012). Structure of the yeast F1Fo-ATP synthase dimer and its role in shaping the mitochondrial cristae. *Proc. Natl. Acad. Sci. USA* *109*, 13602–13607.
- Duckles, S.P., Krause, D.N., Stirone, C., and Procaccio, V. (2006). Estrogen and mitochondria: a new paradigm for vascular protection? *Mol. Interv.* *6*, 26–35.
- Echaniz-Laguna, A., Chassagne, M., Ceresuela, J., Rouvet, I., Padet, S., Acquaviva, C., Nataf, S., Vinzio, S., Bozon, D., and Mousson de Camaret, B. (2012). Complete loss of expression of the ANT1 gene causing cardiomyopathy and myopathy. *J. Med. Genet.* *49*, 146–150.
- Eichner, L.J., and Giguere, V. (2011). Estrogen related receptors (ERRs): a new dawn in transcriptional control of mitochondrial gene networks. *Mitochondrion* *11*, 544–552.
- Fan, W., Waymire, K., Narula, N., Li, P., Rocher, C., Coskun, P.E., Vannan, M.A., Narula, J., MacGregor, G.R., and Wallace, D.C. (2008). A mouse model of mitochondrial disease reveals germline selection against severe mtDNA mutations. *Science* *319*, 958–962.
- Freeman, H.C., Hugill, A., Dear, N.T., Ashcroft, F.M., and Cox, R.D. (2006). Deletion of nicotinamide nucleotide transhydrogenase: a new quantitative trait locus accounting for glucose intolerance in C57BL/6J mice. *Diabetes* *55*, 2153–2156.
- Geyer, H., Caracciolo, G., Abe, H., Wilansky, S., Carerj, S., Gentile, F., Nesser, H.J., Khandheria, B., Narula, J., and Sengupta, P.P. (2010). Assessment of myocardial mechanics using speckle tracking echocardiography: fundamentals and clinical applications. *J. Am. Soc. Echocardiogr.* *23*, 351–369, quiz 453–355.
- Glytsou, C., Calvo, E., Cogliati, S., Mehrotra, A., Anastasia, I., Rigoni, G., Raimondi, A., Shintani, N., Loureiro, M., Vazquez, J., et al. (2016). Optic atrophy 1 is epistatic to the core MICOS component MIC60 in mitochondrial cristae shape control. *Cell Rep.* *17*, 3024–3034.
- Graham, B.H., Waymire, K.G., Cottrell, B., Trounce, I.A., MacGregor, G.R., and Wallace, D.C. (1997). A mouse model for mitochondrial myopathy and cardiomyopathy resulting from a deficiency in the heart/skeletal muscle isoform of the adenine nucleotide translocator. *Nat. Genet.* *16*, 226–234.
- Gray, J.J., Zommer, A.E., Bouchard, R.J., Duval, N., Blackstone, C., and Linseman, D.A. (2013). N-terminal cleavage of the mitochondrial fusion GTPase OPA1 occurs via a caspase-independent mechanism in cerebellar granule neurons exposed to oxidative or nitrosative stress. *Brain Res.* *1494*, 28–43.
- Houtkooper, R.H., Argmann, C., Houten, S.M., Canto, C., Jenning, E.H., Andreux, P.A., Thomas, C., Doenlen, R., Schoonjans, K., and Auwerx, J. (2011). The metabolic footprint of aging in mice. *Sci. Rep.* *1*, 134.
- Huang, T.T., Naeemuddin, M., Elchuri, S., Yamaguchi, M., Kozy, H.M., Carlson, E.J., and Epstein, C.J. (2006). Genetic modifiers of the phenotype of mice deficient in mitochondrial superoxide dismutase. *Hum. Mol. Genet.* *15*, 1187–1194.
- Jang, J.Y., Choi, Y., Jeon, Y.K., Aung, K.C., and Kim, C.W. (2008). Overexpression of adenine nucleotide translocase 1 (ANT1) induces apoptosis and tumor regression in vivo. *BMC Cancer* *8*, 160.
- Ji, F., Sharpley, M.S., Derbeneva, O., Alves, L.S., Qian, P., Wang, Y., Chalkia, D., Lvova, M., Xu, J., Yao, W., et al. (2012). Mitochondrial DNA variant associated with Leber hereditary optic neuropathy and high-altitude Tibetans. *Proc. Natl. Acad. Sci. USA* *109*, 7391–7396.
- Ji, Y., Liang, M., Zhang, J., Zhang, M., Zhu, J., Meng, X., Zhang, S., Gao, M., Zhao, F., Wei, Q.P., et al. (2014). Mitochondrial haplotypes may modulate the phenotypic manifestation of the LHON-associated ND1 G3460A mutation in Chinese families. *J. Hum. Genet.* *59*, 134–140.
- Kim, A., Chen, C.H., Ursell, P., and Huang, T.T. (2010). Genetic modifier of mitochondrial superoxide dismutase-deficient mice delays heart failure and prolongs survival. *Mamm. Genome* *21*, 534–542.
- Kokoszka, J.E., Waymire, K.G., Flierl, A., Sweeney, K.M., Angelin, A., MacGregor, G.R., and Wallace, D.C. (2016). Deficiency in the mouse mitochondrial adenine nucleotide translocator isoform 2 gene is associated with cardiac noncompaction. *Biochim. Biophys. Acta* *1857*, 1203–1212.
- Kokoszka, J.E., Waymire, K.G., Levy, S.E., Sligh, J.E., Cai, J., Jones, D.P., MacGregor, G.R., and Wallace, D.C. (2004). The ADP/ATP translocator is not essential for the mitochondrial permeability transition pore. *Nature* *427*, 461–465.
- Lin, C.S., Sharpley, M.S., Fan, W., Waymire, K.G., Sadun, A., Carelli, V., Ross-Cisneros, F.N., Baci, P., Sung, E., McManus, M.J., et al. (2012). A mouse mtDNA mutant model of Leber's hereditary optic neuropathy. *Proc. Natl. Acad. Sci. USA* *109*, 20065–20070.
- McManus, M.J., Murphy, M.P., and Franklin, J.L. (2014). Mitochondria-derived reactive oxygen species mediate caspase-dependent and -independent neuronal deaths. *Mol. Cell. Neurosci.* *63*, 13–23.
- Mofarrah, M., Guo, Y., Haspel, J.A., Choi, A.M., Davis, E.C., Gouspillou, G., Hepple, R.T., Godin, R., Burelle, Y., and Hussain, S.N. (2013). Autophagic flux and oxidative capacity of skeletal muscles during acute starvation. *Autophagy* *9*, 1604–1620.
- Morrow, R.M., Picard, M., Derbeneva, O., Leipzig, J., McManus, M.J., Gouspillou, G., Barbat-Artigas, S., Dos Santos, C., Hepple, R.T., Murdock, D.G., et al. (2017). Mitochondrial energy deficiency leads to hyperproliferation of skeletal muscle mitochondria and enhanced insulin sensitivity. *Proc. Natl. Acad. Sci. USA* *114*, 2705–2710.
- Mourier, A., Ruzzenente, B., Brandt, T., Kuhlbrandt, W., and Larsson, N.G. (2014). Loss of LRPPRC causes ATP synthase deficiency. *Hum. Mol. Genet.* *23*, 2580–2592.
- Murphy, E., Ardehali, H., Balaban, R.S., DiLisa, F., Dorn, G.W., 2nd, Kitsis, R.N., Otsu, K., Ping, P., Rizzuto, R., Sack, M.N., et al. (2016). Mitochondrial function, biology, and role in disease: a scientific statement from the American Heart Association. *Circ. Res.* *118*, 1960–1991.
- Murphy, M.P. (2009). How mitochondria produce reactive oxygen species. *Biochem. J.* *417*, 1–13.
- Narula, N., Zaragoza, M.V., Sengupta, P.P., Li, P., Haider, N., Verjans, J., Waymire, K., Vannan, M., and Wallace, D.C. (2011). Adenine nucleotide translocase 1 deficiency results in dilated cardiomyopathy with defects in myocardial mechanics, histopathological alterations, and activation of apoptosis. *JACC Cardiovasc. Imaging* *4*, 1–10.
- Navarro, S.J., Trinh, T., Lucas, C.A., Ross, A.J., Waymire, K.G., and Macgregor, G.R. (2012). The C57BL/6J mouse strain background modifies the effect of a mutation in Bcl2l2. *G3 (Bethesda)* *2*, 99–102.

- Norton, M., Ng, A.C., Baird, S., Dumoulin, A., Shutt, T., Mah, N., Andrade-Navarro, M.A., McBride, H.M., and Screatton, R.A. (2014). ROMO1 is an essential redox-dependent regulator of mitochondrial dynamics. *Sci. Signal.* 7, ra10.
- Palmer, J.W., Tandler, B., and Hoppel, C.L. (1977). Biochemical properties of subsarcolemmal and interfibrillar mitochondria isolated from rat cardiac muscle. *J. Biol. Chem.* 252, 8731–8739.
- Palmieri, L., Alberio, S., Pisano, I., Lodi, T., Meznaric-Petrusa, M., Zidar, J., Santoro, A., Scarcia, P., Fontanesi, F., Lamantea, E., et al. (2005). Complete loss-of-function of the heart/muscle-specific adenine nucleotide translocator is associated with mitochondrial myopathy and cardiomyopathy. *Hum. Mol. Genet.* 14, 3079–3088.
- Patten, D.A., Wong, J., Khacho, M., Soubannier, V., Mailloux, R.J., Pilon-Larose, K., MacLaurin, J.G., Park, D.S., McBride, H.M., Trinkle-Mulcahy, L., et al. (2014). OPA1-dependent cristae modulation is essential for cellular adaptation to metabolic demand. *EMBO J.* 33, 2676–2691.
- Paumard, P., Vaillier, J., Couly, B., Schaeffer, J., Soubannier, V., Mueller, D.M., Brethes, D., di Rago, J.P., and Velours, J. (2002). The ATP synthase is involved in generating mitochondrial cristae morphology. *EMBO J.* 21, 221–230.
- Picard, M., McManus, M.J., Csordas, G., Varnai, P., Dorn II, G.W., Williams, D., Hajnoczky, G., and Wallace, D.C. (2015). Trans-mitochondrial coordination of cristae at regulated membrane junctions. *Nat. Commun.* 6, 6259.
- Porter, G.A., Jr., Hom, J., Hoffman, D., Quintanilla, R., de Mesy Bentley, K., and Sheu, S.S. (2011). Bioenergetics, mitochondria, and cardiac myocyte differentiation. *Prog. Pediatr. Cardiol.* 31, 75–81.
- Ramonet, D., Perier, C., Recasens, A., Dehay, B., Bove, J., Costa, V., Scorrano, L., and Vila, M. (2013). Optic atrophy 1 mediates mitochondria remodeling and dopaminergic neurodegeneration linked to complex I deficiency. *Cell Death Differ.* 20, 77–85.
- Scialo, F., Sriram, A., Fernandez-Ayala, D., Gubina, N., Lohmus, M., Nelson, G., Logan, A., Cooper, H.M., Navas, P., Enriquez, J.A., et al. (2016). Mitochondrial ROS produced via reverse electron transport extend animal lifespan. *Cell Metab.* 23, 725–734.
- Strauss, K.A., Dubiner, L., Simon, M., Zaragoza, M., Sengupta, P.P., Li, P., Narula, N., Dreike, S., Platt, J., Procaccio, V., et al. (2013). Severity of cardiomyopathy associated with adenine nucleotide translocator-1 deficiency correlates with mtDNA haplogroup. *Proc. Natl. Acad. Sci. USA* 110, 3253–3458.
- Strauss, M., Hofhaus, G., Schroder, R.R., and Kuhlbrandt, W. (2008). Dimer ribbons of ATP synthase shape the inner mitochondrial membrane. *EMBO J.* 27, 1154–1160.
- Tiepolo, T., Angelin, A., Palma, E., Sabatelli, P., Merlini, L., Nicolosi, L., Finetti, F., Braghetta, P., Vuagniaux, G., Dumont, J.M., et al. (2009). The cyclophilin inhibitor Debio 025 normalizes mitochondrial function, muscle apoptosis and ultrastructural defects in Col6a1<sup>-/-</sup> myopathic mice. *Br. J. Pharmacol.* 157, 1045–1052.
- Toye, A.A., Lippiat, J.D., Proks, P., Shimomura, K., Bentley, L., Hugill, A., Mijat, V., Goldsworthy, M., Moir, L., Haynes, A., et al. (2005). A genetic and physiological study of impaired glucose homeostasis control in C57BL/6J mice. *Diabetologia* 48, 675–686.
- van der Westhuizen, F.H., Smet, J., Levanets, O., Meissner-Roloff, M., Louw, R., Van Coster, R., and Smuts, I. (2010). Aberrant synthesis of ATP synthase resulting from a novel deletion in mitochondrial DNA in an African patient with progressive external ophthalmoplegia. *J. Inher. Metab. Dis.* 33 (Suppl 3), S55–S562.
- Vermulst, M., Bielas, J.H., Kujoth, G.C., Ladiges, W.C., Rabinovitch, P.S., Prolla, T.A., and Loeb, L.A. (2007). Mitochondrial point mutations do not limit the natural lifespan of mice. *Nat. Genet.* 39, 540–543.
- Vermulst, M., Bielas, J.H., and Loeb, L.A. (2008a). Quantification of random mutations in the mitochondrial genome. *Methods* 46, 263–268.
- Vermulst, M., Wanagat, J., Kujoth, G.C., Bielas, J.H., Rabinovitch, P.S., Prolla, T.A., and Loeb, L.A. (2008b). DNA deletions and clonal mutations drive premature aging in mitochondrial mutator mice. *Nat. Genet.* 40, 392–394.
- Wallace, D.C. (2013a). Bioenergetics in human evolution and disease: implications for the origins of biological complexity and the missing genetic variation of common diseases. *Philos. Trans. R. Soc. Lond. B Biol. Sci.* 368, 20120267.
- Wallace, D.C. (2013b). Mitochondrial bioenergetic etiology of disease. *J. Clin. Invest.* 123, 1405–1412.
- Wittig, I., Karas, M., and Schagger, H. (2007). High resolution clear native electrophoresis for in-gel functional assays and fluorescence studies of membrane protein complexes. *Mol. Cell. Proteomics* 6, 1215–1225.
- Wittig, I., Meyer, B., Heide, H., Steger, M., Bleier, L., Wumaier, Z., Karas, M., and Schagger, H. (2010). Assembly and oligomerization of human ATP synthase lacking mitochondrial subunits a and A6L. *Biochim. Biophys. Acta* 1797, 1004–1011.
- Yadava, N., Potluri, P., Smith, E.N., Bisevac, A., and Scheffler, I.E. (2002). Species-specific and mutant MWFE proteins. their effect on the assembly of a functional mammalian mitochondrial complex I. *J. Biol. Chem.* 277, 21221–21230.
- Yu, T., Sheu, S.S., Robotham, J.L., and Yoon, Y. (2008). Mitochondrial fission mediates high glucose-induced cell death through elevated production of reactive oxygen species. *Cardiovasc. Res.* 79, 341–351.
- Zamora, M., Granel, M., Mampel, T., and Vinas, O. (2004a). Adenine nucleotide translocase 3 (ANT3) overexpression induces apoptosis in cultured cells. *FEBS Lett.* 563, 155–160.
- Zamora, M., Merono, C., Vinas, O., and Mampel, T. (2004b). Recruitment of NF-kappaB into mitochondria is involved in adenine nucleotide translocase 1 (ANT1)-induced apoptosis. *J. Biol. Chem.* 279, 38415–38423.
- Zaragoza, M.V., Brandon, M.C., Diegoli, M., Arbustini, E., and Wallace, D.C. (2011). Mitochondrial cardiomyopathies: how to identify candidate pathogenic mutations by mitochondrial DNA sequencing, MITOMASTER and phylogeny. *Eur. J. Hum. Genet.* 19, 200–207.
- Zorov, D.B., Filburn, C.R., Klotz, L.O., Zweier, J.L., and Sollott, S.J. (2000). Reactive oxygen species (ROS)-induced ROS release: a new phenomenon accompanying induction of the mitochondrial permeability transition in cardiac myocytes. *J. Exp. Med.* 192, 1001–1014.

## STAR★METHODS

### KEY RESOURCES TABLE

REAGENT or RESOURCE	SOURCE	IDENTIFIER
<b>Antibodies</b>		
Mouse monoclonal anti-VDAC	Abcam	Cat#ab14734; RRID: AB_443084
Rabbit monoclonal anti-VDAC	Cell Signaling Technology	Cat#D73D12; RRID: AB_10557420
Mouse Monoclonal total OXPPOS rodent antibody cocktail	Abcam	Cat#ab110413; RRID: AB_2629281
Mouse monoclonal anti-NDUFA1	<a href="#">Yadava et al., 2002</a>	N/A
Mouse monoclonal anti-OPA1	BD Biosciences	Cat#612606; RRID: AB_399888
Fluorescent TrueBlot: Anti-Mouse Ig DyLight 800	Rockland	Cat#18-4517-32; RRID: AB_2610842
Rabbit IgG (H&L) Antibody DyLight 800 Conjugated Pre-Adsorbed	Rockland	Cat#611-145-122; RRID: AB_1057618
<b>Critical Commercial Assays</b>		
Ion Total RNA-Seq Kit v.2	Life Technologies	Cat#4475936
Ion PI Sequencing 200 Kit v.2 chemistry	Life Technologies	Cat#4485149
PureLink RNA-Easy kit	Life Technologies	Cat#12183018A
RiboMinus Eukaryote System v.2	Life Technologies	Cat #A15026
OxiSelect Nitrotyrosine ELISA Kit	Cell Biolabs	Cat#STA-305
CaspaseGlo 3/7	Promega	Cat#G8090
<b>Deposited Data</b>		
Raw sequence files and associated metadata	This paper	SRA: SUB2425516
Reproducible code for generating the values presented in this paper	This paper	<a href="https://github.com/chop-dbhi/mcmanus_ant1">https://github.com/chop-dbhi/mcmanus_ant1</a>
<b>Experimental Models: Organisms/Strains</b>		
Mouse: WT: C57Bl/6J	<a href="#">Navarro et al., 2012</a>	N/A
Mouse: COI: <i>COI</i> <sup>V421A</sup> C57Bl/6J	This paper	N/A
Mouse: ND6: <i>ND6</i> <sup>P25L</sup> C57Bl/6J	This paper	N/A
Mouse: ANT1: <i>Ant1</i> <sup>-/-</sup> C57Bl/6J	<a href="#">Morrow et al., 2017</a>	N/A
Mouse: ANT1/COI: <i>Ant1</i> <sup>-/-</sup> , <i>COI</i> <sup>V421A</sup> C57Bl/6J	This paper	N/A
Mouse: ANT1/ND6: <i>Ant1</i> <sup>-/-</sup> , <i>ND6</i> <sup>P25L</sup> C57Bl/6J	This paper	N/A
<b>Oligonucleotides</b>		
Primers for mtDNA LT-PCR ND2 Forward: 5'CTGGAA TTCAGCCTACTAGCAATTATCC-3'; 12s Reverse: 5'-TTTAGGTTTATGGCTAAGCATAGTGGG- 3'	This paper	N/A
Primers for mtDNA deletions flanking multiple TaqI restriction sites: Deletion Forward: 5'-AGGCCAC CACTCCTATTG-3', position 8810-8829; Deletion Reverse: 5'-AATGCTAGGCGTTTGATTGG-3', position 13098-13117	<a href="#">Vermulst et al., 2008b</a>	N/A
Primers for mtDNA Taq1 controls: Control Forward: 5'-TCGGCGTAAAACGTGCAAC-3', position 350-369; Control Reverse: 5'-CCGCCAAGTCCTTTGAGTTT-3' position 579-598	<a href="#">Vermulst et al., 2008b</a>	N/A
<b>Software and Algorithms</b>		
Speckle tracking echocardiography: Vevostrain software	Visual Sonics	<a href="https://www.visualsonics.com/product/software/vevo-lab">https://www.visualsonics.com/product/software/vevo-lab</a>
Electron micrograph quantification: Image J	National Institutes of Health	<a href="https://imagej.nih.gov/ij/download.html">https://imagej.nih.gov/ij/download.html</a>
Western Analysis: Image Studio	LI-COR	<a href="https://www.licor.com/bio/products/software/image_studio_lite/">https://www.licor.com/bio/products/software/image_studio_lite/</a>

## CONTACT FOR REAGENT AND RESOURCE SHARING

Further information and requests for resources and reagents should be directed to and will be fulfilled by the Lead Contact, Douglas C. Wallace ([wallaced1@email.chop.edu](mailto:wallaced1@email.chop.edu)).

## EXPERIMENTAL MODEL AND SUBJECT DETAILS

### Mouse Genetics

All mice were maintained on the C57Bl/6J background, which was derived from the Jackson Laboratory C56Bl/6J line into which the wild-type (WT) nicotinamide nucleotide transhydrogenase (*Nnt*) gene was reintroduced (Navarro et al., 2012), herein designated as WT. These mice were compared to mice harboring the mtDNA NADH dehydrogenase subunit 6 gene (*ND6*) nt 13997G>A P25L or cytochrome c oxidase subunit I gene (*COI*) nt 6598T>C V421 mutations generated via the female embryonic stem (ES) cell fusion method (Fan et al., 2008; Lin et al., 2012). The phenotypes of these mtDNA variants, as well as the adenine nucleotide translocator isoform 1 (*Ant1*)-null gene (Graham et al., 1997; Narula et al., 2011), were previously reported on the C56Bl/6J *Nnt*<sup>-/-</sup> strain. We transferred the *Ant1*<sup>-/-</sup>, *ND6*<sup>P25L</sup>, and *COI*<sup>V421A</sup> mutations in to the C57Bl/6J strain by repeated backcrosses to remove the confounding influence of the nuclear modifier, *Nnt* (Huang et al., 2006; Kim et al., 2010). The C57Bl/6J *Ant1*<sup>-/-</sup> males were then crossed with female C57Bl/6J *ND6*<sup>P25L</sup> or *COI*<sup>V421A</sup> to attain C57Bl/6J *Ant1*<sup>-/-</sup> *ND6*<sup>P25L</sup> and C57Bl/6J *Ant1*<sup>-/-</sup> *COI*<sup>V421A</sup> mice. The WT and *Ant1*<sup>-/-</sup> mice were maintained by brother-sister matings. The mtDNA *ND6*<sup>P25L</sup> and *COI*<sup>V421A</sup> mutant mice were maintained by crossing female mtDNA mutant mice with WT males. The *Ant1*<sup>-/-</sup> *ND6*<sup>P25L</sup> and *Ant1*<sup>-/-</sup> *COI*<sup>V421A</sup> mutant mice were maintained by crossing the *Ant1*<sup>-/-</sup> *ND6*<sup>P25L</sup> and *Ant1*<sup>-/-</sup> *COI*<sup>V421A</sup> females with *Ant1*<sup>-/-</sup> males.

### Mouse Maintenance and Longevity

All experimental procedures involving mice were conducted in accordance to approved Institutional Animal Care and Use Committee (IACUC) protocols at the Children's Hospital of Philadelphia. To eliminate confounding effects of estrogen on mitochondrial physiology, only male mice were considered in our analyses (Duckles et al., 2006; Eichner and Giguere, 2011). Male mice were pooled at weaning to attain 3 – 5, genotype-, sex- and age-matched mice per cage with *ad libitum* access to food and water, on a 13:11 light:dark cycle. A minimum of 3 subjects per strain were used for all experiments, except assessment of respiratory complex I assembly by blue-native electrophoresis (n = 2). Additional subjects were included, as noted, based on the availability of age- and strain- matched mice and nature of the assay (Lin et al., 2012; Narula et al., 2011). During sample preparation, subjects were randomly numbered to blind the experimenter for subsequent tests and analysis. The effect of specific mitochondrial genetic variation on longevity was determined by Kaplan–Meier survival curves constructed from the known date of birth and death of at least one hundred mice per genotype. Apart from cage changes and daily health checks, these mice were left undisturbed. When mice were determined moribund by the veterinary staff, they were humanely euthanized and the date of death recorded. Differences between groups were evaluated using the log-rank (Mantel-Cox) test (GraphPad, La Jolla, CA, USA).

## METHOD DETAILS

### RNA Sequencing and Bioinformatics

Total RNA was extracted in Trizol with a motorized pestle from 30–60 mg of left myocardium (n = 4) and processed with the PureLink RNA-Easy kit (Life technologies #12183018A), and affinity-depleted of ribosomal RNA (rRNA) with magnetic bead RiboMinus Eukaryote System v2 (Life technologies # A15026). PolyA enrichment was avoided to maximize recovery of mtDNA-encoded transcripts. Purified RNA was quantified and quality checked with RNA 6000 Pico chip (Agilent #5067-1513) on Agilent Bioanalyzer 2100, and spiked with the ERCC RNA Spike-In Mix (4456740). Library preparation was performed from 800 ng of rRNA-depleted RNA and processed with the Ion Total RNA-Seq Kit v2 (Life technologies #4475936) and multiplexed-sequenced with Ion PI Sequencing 200 Kit v2 chemistry (Life Technologies #4485149) on the Ion Proton platform. Two samples were pooled per chip, yielding on average >25 million reads per sample, and an average read length of ~80 bp. After trimming, transcript counts were generated by a STAR alignment to the reference mouse genome, mapping to a total of 14,642 annotated genes, and normalized using ERCC spike-ins counts. Differential expression, fold change, and statistical significance for each gene was established using the DESeq Bioconductor package in R. DESeq. Data were subsequently analyzed for individual genes of interest, or using DAVID (Database for Annotation, Visualization and Integrated Discovery v6.7) to derive functional significance of up- and down-regulated pathways of interest.

### Cardiac Size and Histopathology

Hearts were excised, weighed, and fixed in 4% paraformaldehyde for at least 48 hr. Relative heart weight was determined by the ratio of heart to body weight over the lifespan of each strain (n = 65 – 111). Longitudinal sections of paraffin embedded tissues were sliced and stained with hematoxylin and eosin stain (H&E; n = 3).

### Calorimetry

Energy expenditure was assessed using indirect calorimetry (Oxymax; Columbus Instruments). Mice were singly housed with water and food ad libitum ( $n = 6$ ). After a 3-day acclimation period, oxygen consumption and carbon dioxide production were measured over 30 hr using an air flow of 600 mL/min at 22°C. For the cold stress challenge, mice were placed in 4°C for 6 hr. Core body temperature was measured using a rectal probe (Harvard Apparatus).

### Speckle Tracking Echocardiography of Left Ventricular Mechanics

Images were obtained using the Vevo2100 equipped with a MS550D transducer (Visual Sonics, Toronto, ON, Canada). The mice were lightly anaesthetized using 1.5% isoflurane mixed with 100% O<sub>2</sub> during the time of imaging. Electrocardiography leads were applied to monitor heart rate and trigger echo image acquisitions. The images were obtained from the B-mode long-axis view and the M-mode of the parasternal short-axis view. Speckle tracking echocardiography (STE) was performed as a sensitive indicator of myocardial contractility using Vevostrain software (Visual Sonics, Toronto, ON, Canada) incorporated into the Vevo2100 from the movies acquired from the B-mode long-axis view. The tracking quality was visually inspected, and the tracing was confirmed as acceptable when the traced line moved along with the moving heart image for at least three cardiac cycles. These cardiac cycles were used for the analysis. Strain analysis was performed using speckle tracking algorithms applied on high-frequency ultrasound images. Parasternal long-axis view provided longitudinal strain, whereas, parasternal short axis view was used for assessing circumferential strain. M-mode images at mid-LV were used to determine left ventricular internal dimension at end-diastole (LVIDd) and LV dimension internal dimension at end-systole (LVIDs). The LV ejection fraction (EF) was calculated. Interventricular septum (IVS) wall thickness and left ventricular posterior wall (LVPW) thickness were obtained ( $n = 10 - 34$ ).

### Mitochondrial Morphology

Thin slices of left ventricular myocardium were excised from 6 month old animals of each genotype and immediately immersed in fixation buffer containing 2% glutaraldehyde and 0.1 M cacodylate (pH 7.4) (Picard et al., 2015). Samples were post-fixed in 2.0% osmium tetroxide for 1 h at room temperature and rinsed in distilled H<sub>2</sub>O before in-bloc staining with 2% uranyl acetate. After dehydration through a graded ethanol series, each sample was embedded in EMBED-812 (Electron Microscopy Sciences, Fort Washington, PA). Cardiomyocyte orientation and quality were first checked in 1  $\mu$ m thick sections stained with 1% toluidine blue. Thin sections (90  $\mu$ m) were then mounted on filmed copper grids and stained with uranyl acetate and lead citrate and examined on a JEOL 1010 electron microscope fitted with a Hamamatsu digital camera and AMT Advantage image capture software. Myocardial mitochondria were manually traced from at least 8 calibrated images per subject at x12,000 indirect magnification using Image J (National Institutes of Health, Bethesda, MD). To produce frequency distributions of morphological parameters, the area of each mitochondrion was assigned to one of twenty bins of equal size. Lipofuscin granules were counted per image and normalized to the mean of WT. Abnormal mitochondria were counted and expressed as percent of total mitochondria per image. The most common types of cristae defects found across all strains (i.e., reticular, partitioning, circular, concentric, or paracrystalline structures and cristolysis) were manually quantified. Statistical significance was evaluated based on 95% confidence interval (C.I.) of the mean.

### Mitochondrial Isolation

Mitochondria were isolated from murine hearts (Palmer et al., 1977). The entire procedure was performed on ice or in a cold room (4°C). Ventricular tissue was excised, blotted, weighed, rinsed, and diced in a small beaker containing 2 mL of ice-cold organ preservation solution (BIOPS) comprised of 2.77 mM CaK<sub>2</sub> EGTA buffer, 7.23 mM K<sub>2</sub> EGTA buffer, 0.1  $\mu$ M free calcium, 20 mM imidazole, 20 mM taurine, 50 mM 2-(N-morpholino) ethanesulfonic acid hydrate (MES), 0.5 mM dithiothreitol, 6.56 mM MgCl<sub>2</sub> · 6H<sub>2</sub>O, 5.77 mM ATP, and 15 mM phosphocreatine (pH 7.1). The buffer was decanted, and tissue digested in 0.015% trypsin for 10 min. The protease was neutralized by 5x dilution in isolation buffer (50 mM MOPS, 100 mM KCl, 1 mM EGTA, 5 mM MgSO<sub>4</sub>, 1mM ATP) containing 10 mg/ml fatty acid-free BSA. The tissue was electrically homogenized using a Eurostar Power B (1100 rpm x 7-8 strokes) and mitochondria isolated by differential centrifugation. The final pellet was resuspended in the appropriate experimental buffer.

### Complex I Activity

Complex I NADH-ubiquinone reductase (NQR) activity (Ji et al., 2014) was assayed using 25  $\mu$ g/ml of isolated mitochondria using the complex I assay buffer (250 mM sucrose, 10 mM Hepes, 0.2 mM EDTA, 2.5 mM MgCl<sub>2</sub>, pH 7.2) containing 40  $\mu$ g/mL alamethicin to permeabilize the mitochondria inner membrane. After 1 min, the reaction was started by addition of 100  $\mu$ M coenzyme Q<sub>1</sub>, and 200  $\mu$ M NADH. NADH oxidation was monitored at 340 nm using a Cary300 dual-beam spectrophotometer at 30°C, and rotenone sensitive activity calculated. NQR activity was determined by subtracting the basal (no substrate) and the rotenone (4  $\mu$ M) insensitive rates from the NADH:CoQ<sub>1</sub> rate. The results are shown as nmol NADH mg<sup>-1</sup> min<sup>-1</sup> using the extinction coefficient of NADH at 340 nm (6.22 mM<sup>-1</sup> cm<sup>-1</sup>). The assay was performed in 3 independent trials ( $n = 3 - 7$ ).

The amount of assembled complex I was estimated by assaying diaphorase-type activity from complex I immunocaptured from isolated heart mitochondria (10  $\mu$ g/ml) (Abcam; ab109721). The assay was performed in 2 independent trials ( $n = 3 - 6$ ).

### Native Gel Electrophoresis and Immunodetection

Mitochondrial respiratory complexes were separated by native electrophoresis for analysis of complex I assembly (Yadava et al., 2002). Fresh mitochondrial pellets equivalent to 400  $\mu$ g of protein were solubilized with 800  $\mu$ g of dodecyl- $\beta$ -D-maltoside

(DDM; Sigma) in 5 mM 6-aminohexanoic acid, 50 mM imidazole-HCl (pH 7.0) and 10% glycerol. Coomassie Brilliant Blue G-250 (Serva) was added to the solubilized samples at a dye/detergent ratio of 1:5 (w/w). The samples were loaded on a 4%–13% acrylamide gradient gel and electrophoresed overnight. Proteins were transferred to PVDF membranes from the native gels and western blotting performed using standard transfer conditions for 3 hr. The blots were de-stained by washing with 100% methanol and then probed with NDUFA1 antisera to determine complex I assembly ( $n = 5$ ; antibody provided by Scheffler IE; validated in (Yadava et al., 2002)).

The assembly and oligomerization state of  $F_1F_0$  ATPase were determined using clear native electrophoresis (CNE) (Wittig et al., 2007). To quantify the holo-complex V ( $V_m$ ) stability, mitochondrial protein was solubilized on ice for 15 min with 2.5% DDM. The samples were then centrifuged for 30 min at 25000 g, 4°C, and equal mitochondrial protein loaded on CNE gels. The complexes were electrophoresed overnight at 100 – 120 mV; the gel incubated in 35 mM Tris (0.42%), 270 mM Glycine (2.02%), pH 8.3 for 2h; and washed in the same buffer supplemented with 14 mM  $MgSO_4$ , 0.2%  $Pb(NO_3)_2$ , and 8 mM ATP until the white lead phosphate precipitated. The reaction was stopped with 50% methanol, and the gel imaged. Western blots of duplicate gels were probed with an anti-mouse VDAC monoclonal antibody as a loading control (Abcam; ab14734). The assay was performed in 4 independent trials ( $n = 4$ ).

### Cytochrome-c Oxidase and Citrate Synthase Activity

Frozen samples from the left ventricular myocardium were thawed on ice and approximately 10 mg of each was diced and homogenized with a Teflon pestle at 1:30 (w/v) in 50 mM triethanolamine with 1 mM EDTA (pH 7.4). The samples were solubilized in potassium phosphate buffer and 0.1% (w/v) n-dodecylmaltoside (pH 7.5). The reaction was started by the addition of 0.1 mM reduced ferrocyanochrome c (0.1 mM) and the initial rate of oxidation determined by following the decrease in absorbance at 550 nm in a 96-well plate at 30°C (Capaldi et al., 1995). To control for differences in myocardial mitochondrial content, citrate synthase (CS) activity was determined from the same tissue homogenates (Mofarrah et al., 2013). The samples were diluted 1:26 in CS buffer (100 mM Tris, 0.2 mM acetylCoA, 0.2 mM 5,5-dithio-bis-2-nitrobenzoic acid (DTNB), 70  $\mu$ M oxaloacetate) and the change in absorbance of DTNB was measured at 412 nm. Parallel samples in buffer lacking oxaloacetate were included as negative controls to ensure specificity of the reaction. The molar extinction coefficients used were 29.5  $L \cdot mol^{-1} \cdot cm^{-1}$  for ferrocyanochrome c and 13.6  $L \cdot mol^{-1} \cdot cm^{-1}$  for DTNB. Each assay was performed twice,  $n = 4 - 6$ .

### Western Blotting and ELISA

Isolated mitochondria were resuspended in 2% SDS (50 mM Tris pH 7.4), rotated at 4°C for 30 min, centrifuged at 16,000  $xg$  for 10min, and the protein concentration of the supernatant determined by the BCA assay. Aliquots, 30  $\mu$ g each, were run through a 4%–12% SDS-PAGE and electroblotted onto a nitrocellulose membrane. The membrane was then probed with anti-OPA1 (Cell Signaling), Total OXPHOS Rodent WB Antibody Cocktail (Abcam; ab110413), or anti-VDAC (Cell Signaling; D73D12) primary antibodies, followed by the appropriate secondary antibody (Fluorescent TrueBlot: Anti-Mouse or Rabbit Ig DyLight 800 (Rockland)), imaged on an Odyssey System, and quantified using Image Studio. Each sample was first normalized to VDAC, and then to the mean of the age-matched WT control,  $n = 3 - 6$ , in four independent experiments.

Nitrotyrosine concentration was measured by enzyme-linked immunosorbent assay (ELISA) using heart tissue homogenate from 12 mo. old animals according to the *OxiSelect Nitrotyrosine ELISA Kit* protocol (STA-305, Cell Biolabs, San Diego, CA, USA),  $n = 3-4$ .

### Respiration

High-resolution respirometry of isolated mitochondria was performed in ice-cold mitochondrial respiration medium 5 (MiR05: 0.5 mM EGTA, 3 mM  $MgCl_2$ , 60 mM potassium lactobionate, 20 mM taurine, 10 mM  $KH_2PO_4$ , 20 mM HEPES, 110 mM sucrose, and 1 g/L BSA essentially fatty acid free, adjusted to pH 7.1) at 25°C using the Oxygraph-2k (Oroboros, Innsbruck, Austria). Sequential oxygen consumption rates were determined in mitochondria respiring first on malate (2 mM) and glutamate (10 mM) (state II;  $L = LEAK$ ), followed by addition of 2.5 mM ADP (state III;  $P$  state), then the addition of oligomycin (2  $\mu$ g/mL) (state 4), and lastly addition of rotenone and antimycin A (residual oxygen consumption; ROX). The quality of the mitochondrial preparations was confirmed by the absence of a cytochrome c effect on oxygen consumption in the  $P$  state (data not shown). Respirometry experiments were conducted in pairs of over 18 independent experiments,  $n = 3$ .

### Mitochondrial Reactive Oxygen Species (mtROS) and Membrane Potential (MMP)

The rate of mtROS production was determined by monitoring the oxidation of the fluorogenic indicator Amplex Red by  $H_2O_2$  in the presence of horseradish peroxidase as previously described (Lin et al., 2012). Mitochondria (0.05 mg/ml) were incubated in assay medium [125 mM KCl, 20 mM Hepes, 2 mM  $K_2HPO_4$ , 1 mM  $MgCl_2$ , 0.1 mM EGTA, 0.025% BSA (pH 7.2) at 37°C]. Glutamate and malate (5 mM each) were used to induce forward electron transport. For reverse electron transport experiments, 5 mM succinate and 1  $\mu$ g/ml oligomycin were included. Amplex Red (1  $\mu$ M) and 5 U  $\cdot$  mL<sup>-1</sup> horseradish peroxidase were added to initiate the reaction. Fluorescence was recorded at excitation 560 nm and emission 590 nm. Mitochondrial membrane potential (MMP) was assessed on 0.025 mg mitochondria using the potentiometric fluorescent dye TMRM (100 nM) (535 nm excitation, 600 nm emission) while metabolizing the complex I substrates malate and glutamate. The results were normalized by comparison with a parallel experiment but with the FCCP (carbonyl cyanide-4-(trifluoromethoxy) phenylhydrazone) uncoupler added. Each sample was run in triplicate,  $n = 3$ , in two independent experiments, and results are shown as fold change from WT per condition.

### Calcium Retention Capacity

The mitochondrial calcium retention capacity (CRC) of mitochondrial preparations (Tiepolo et al., 2009) was assessed by monitoring  $\text{Ca}^{2+}$  uptake and release using the  $\text{Ca}^{2+}$  indicator, Calcium Green-5N (1  $\mu\text{M}$ ; excitation, 505 nm; emission, 535 nm), monitored using a Fluoromax spectrofluorometer (Horiba; Kyoto Japan) equipped with magnetic stirring rod. The incubation medium contained 0.2 M sucrose, 10 mM Tris-MOPS, 5 mM glutamate-Tris, 2.5 mM malate-Tris, 1 mM. Final volume was 2 mL, pH 7.4, 25°C. All the experiments were started with the addition of 0.5 mg/ml mitochondria followed 1 min later by the indicated pulses of  $\text{Ca}^{2+}$ . Each sample was run in duplicate. Traces are representative for the group (n = 3 - 4).

### mtDNA Deletion Analysis

Whole genomic DNA was isolated from the ventricular myocardium using phenol-chloroform-isoamyl alcohol extraction and diluted to 2.5 ng/ $\mu\text{l}$ . mtDNA deletions were detected by amplification of a 12.8 kB mtDNA fragment using Accuprime Hi Fi (Invitrogen 12346068) and the following primer pairs: ND2 Forward: 5'-CTGGAATTCAGCCTACTAGCAATTATCC-3'; 12s Reverse: 5'-TTTAGGTTTATGGCTAAGCATAGTGGGG-3'. The long template PCR products were equally loaded and run in 2 TBE (0.8%) gels and the number of bands per sample (n = 4 - 6) quantified by ImageJ.

To quantify the deletion burden at a particular site, the random mutation capture (RMC) assay was adapted to detect large deletions in the major arc between two 15-bp direct repeats previously shown to be hotspots for mtDNA deletions (Vermulst et al., 2007, 2008a, 2008b). Briefly, mtDNA was first digested by Taq1 to remove WT mtDNA. The number of mtDNA molecules with a deletion were then determined using the following qPCR primers, spaced several kb apart, flanking multiple TaqI restriction sites: Deletion Forward: 5'-AGGCCACCACACTCCTATTG-3', position 8810-8829; Deletion Reverse: 5'-AATGCTAGGCGTTTGATTGG-3', position 13098-13117. The total number of mtDNA molecules per sample was determined using the following control primers that do not include a TaqI site: Control Forward: 5'-TCGGCGTAAAACGTGCAAC-3', position 350-369; Control Reverse: 5'-CCGCCAAGTCCTTTGAGTTT-3' position 579-598. The ratio of deleted mtDNA molecules to total mtDNA molecules was used to determine the deletion frequency in the myocardium of mice 4 - 25 mo. of age. The assay was performed in two independent experiments, n = 8 - 14.

### Caspase-3/7 Activity

To detect caspase-3/7 activity, mouse hearts were homogenized in hypotonic extraction buffer (25 mM HEPES [pH 7.5], 5 mM  $\text{MgCl}_2$ , 1 mM EGTA) on ice. The homogenates were cleared by centrifugation at 13,000 rpm for 15 min at 4°C. Protein concentrations were adjusted to 1 mg/ml, and an equal volume of 10  $\mu\text{g}/\text{ml}$  added to the Caspase-Glo Reagent (Promega G8091). The assays were incubated for 1 hr at room temperature before reading on a luminometer (SpectraMax Paradigm; Eugene, OR). n = 4, performed in two independent experiments.

### COX-SDH Histochemistry

To identify mitochondrial respiratory chain-deficient cardiomyocytes, we performed sequential cytochrome c oxidase (COX) and succinate dehydrogenase (SDH) reactions on frozen sections from the myocardium of mice at 6 and 18 mo. of age. Tissue samples were frozen in isopentane/liquid nitrogen. Cryostat sections were then stained for simultaneous COX and SDH activity and imaged on a Zeiss Axio Imager.M2, using the 20x objective.

### DATA AND SOFTWARE AVAILABILITY

Raw sequence files and associated metadata have been deposited in NCBI SRA: SUB2425516. Reproducible code for generating the values presented in this paper is located at [https://github.com/chop-dbhi/mcmanus\\_ant1](https://github.com/chop-dbhi/mcmanus_ant1).

### QUANTIFICATION AND STATISTICAL ANALYSIS

The data were quantified in Prism 6.0 (GraphPad, La Jolla, CA, USA), and the appropriate statistical analysis performed using one-way or two-way ANOVAs, corrected for multiple comparisons by the Sidak post hoc test, unless noted otherwise. The Brown-Forsythe test was used to determine differences in standard deviations among groups, and the Geisser-Greenhouse correction applied for sphericity. Further statistical details of experiments can be found in the figure legend and results sections.